HHS Public Access

Author manuscript

Science. Author manuscript; available in PMC 2019 March 07.

Published in final edited form as:

Science. 2018 September 07; 361(6406): . doi:10.1126/science.aan8821.

Induced Adult Neurogenesis plus BDNF Mimicks the Effects of Exercise on Cognition in an Alzheimer's Mouse Model

Se Hoon Choi[1], **Enjana Bylykbashi**[1], **Zena K. Chatila**[1], **Star W. Lee**[2], **Benjamin Pulli**[3], **Gregory D. Clemenson**[2], **Eunhee Kim**[1], **Alexander Rompala**[1], **Mary K. Oram**[1], **Caroline Asselin**[1], **Jenna Aronson**[1], **Can Zhang**[1], **Sean J. Miller**[1], **Andrea Lesinski**[1], **John W. Chen**[3], **Doo Yeon Kim**[1], **Henriette van Praag**[4], **Bruce M. Spiegelman**[5], **Fred H. Gage**[2], and **Rudolph E. Tanzi**[1,*]

[1]Genetics and Aging Research Unit, Department of Neurology, Massachusetts General Hospital, Harvard Medical School, Charlestown, Massachusetts 02129, USA.

[2]Laboratoy of Genetics, The Salk Institute for Biological Studies, La Jolla, California 92037, USA

[3]Institute for Innovation in Imaging, Department of Radiology, Massachusetts General Hospital, Boston, Massachusetts 02114, USA.

[4]Department of Biomedical Science, Charles E. Schmidt College of Medicine, and Brain Institute, Florida Atlantic University, Jupiter, Florida 33458, USA.

[5]Department of Cancer Biology, Dana-Farber Cancer Institute, Boston, Massachusetts 02115, USA.

Abstract

Adult hippocampal neurogenesis (AHN) is impaired prior to the onset of Alzheimer's disease (AD) pathology. We found that exercise provided cognitive benefit to 5×FAD mice, a mouse model of AD, by inducing AHN and elevating levels of brain-derived neurotrophic factor (BDNF). Neither stimulation of AHN alone, nor exercise, in the absence of increased AHN, ameliorated cognition. We successfully mimicked the beneficial effects of exercise on AD mice by genetically and pharmacologically inducing AHN in combination with elevating BDNF levels. Suppressing AHN later led to worsened cognitive performance and loss of pre-existing dentate neurons. Thus, pharmacological mimetics of exercise, enhancing AHN and elevating BDNF levels, may improve

*Correspondence to: Rudolph E. Tanzi (tanzi@helix.mgh.harvard.edu).

Zena K. Chatila - Department of Neuroscience, Columbia University, New York, New York, 10036, USA

Star Lee - Department of Evolution, Ecology, and Organismal Biology, University of California, Riverside, Riverside, California 92521, USA

Gregory Clemenson - Department of Neurobiology and Behavior, University of California, Irvine, Irvine, California 92697, USA

Jenna Aronson - Department of Brain and Cognitive Sciences, MIT, Cambridge, MA, USA.

Sean J. Miller - Department of Neurology and Neurological Sciences, School of Medicine, Stanford University, Stanford, CA 94305, USA

Andrea Lesinski - Cell and Molecular Biology, University of Rhode Island, Kingston, RI 02881

Author contributions: R.E.T. and S.C. initiated project; R.E.T. supervised research; R.E.T., S.C., F.H.G., H.vP., and B.M.S. designed experiments; S.C., E.B., Z.K.C., C.A., and M.O. performed most of research; S.W.L.,G.D.C., and F.H.G. provided LV-Wnt3, LV-dnWnt, and LV-GFP; S.C. performed stereotaxic injections; B.P. and J.W.C. performed irradiation; E.B. and J.A., and D.K. performed 3D culture experiments; E.K. and A.R. performed Golgi staining, dot-blot, and ELISAs; M.O. and A.L. genotyped and maintained mice; C.Z. and S.J.M. performed MSD assays; and S.C. E.B., Z.K.C., and R.E.T. wrote manuscript with editing and input from J.W.C., H.vP., and F.H.G.

Competing interest: We declare no conflict of interest.

cognition in AD. Furthermore, applied at early stages of AD, these mimetics may protect against subsequent neuronal cell death.

One Sentence Summary:

Role of Adult Neurogenesis in Alzheimer's Disease.

Alzheimer's disease (AD) is the most common form of age-related dementia, characterized by cognitive impairment, neurodegeneration, deposition of β-amyloid (Aβ), neurofibrillary tangle formation, and neuroinflammation (1). The most popular therapeutic approach aimed at reducing Aβ burden has not yet proven effective in halting disease progression. A successful therapy would ideally both remove the pathological hallmarks of the disease and provide a level of functional recovery.

The human hippocampus contains neural progenitor cells (NPCs) that continue to generate new neurons, a process known as adult hippocampal neurogenesis (AHN) (2). Although adult-generated neurons play an important role in learning and memory under physiological conditions, their function under pathological conditions, such as those of AD, has remained elusive. Emerging evidence indicates that AHN is impaired prior to the onset of classical AD pathology in AD mouse models, e.g., Aβ deposition (3). Human AHN has also been reported to be altered in AD patients (4–9).

To date, however, the evidence supporting a role for AHN in AD has remained sparse and inconclusive. Two fundamental questions remain: (1) whether AHN could be enhanced and exploited for therapeutic purposes for AD, and (2) whether AHN impairment mediates aspects of AD pathogenesis or is a neuroadaptive response to the complex pathological events of the disease. We set out to address these two questions genetically and pharmacologically in 5×FAD mice (10). We also assessed the role of physical exercise, a known neurogenic stimulus that counteracts various aspects of AD pathology (11–13), and explored whether promoting AHN in conjunction with the salutary biochemical changes that are induced by exercise can ameliorate AD pathology and behavioral symptoms in mice. Finally, we investigated how impairment of AHN contributes to AD pathogenesis and assessed the functional roles of adult-generated neurons in the pathological course of AD.

AHN stimulation with LV-Wnt3 and P7C3 or with exercise

To stimulate AHN, beginning at 2 months of age for 4 or 4.5 months, sedentary 5×FAD mice were injected with P7C3, a compound that enhances NPC survival (14). At the 3-month time point, these mice also received lentivirus expressing Wnt3 (LV-Wnt3) to increase NPC proliferation (15) (Fig. 1, A and B). Control 5×FAD mice were injected with vehicle and lentivirus expressing green fluorescent protein (LV-GFP, referred to as "5×FAD^{CTL}" mice). As an alternative means of inducing AHN, we also tested the effects of exercise on a 5×FAD mice cohort. Successful promotion of AHN with P7C3 and LV-Wnt3 or with exercise was observed in the male and female 5×FAD mice, as determined by immunostaining for doublecortin (DCX)$^{+}$ neurons (Fig. 1, C and D). After completing cognition tasks, mice with similar DCX^{+} cell counts among the 5×FAD mice treated with P7C3 and LV-Wnt3 and the

exercised 5×FAD mice were selected for further study; we included all those with levels higher than the maximum level seen in 5×FAD^{CTL} mice (mice in box in Fig. 1D; see Table S1 for animal numbers in each experimental group and group arrangement explanations). From here on, we refer to the subsets of 5×FAD mice treated with P7C3 and LV-Wnt3 to promote AHN or exercised 5×FAD mice in the box in Fig. 1D as "5×FAD^{ProAHN}" and "5×FAD$^{+AHN(RUN)}$" mice, respectively. Exercised 5×FAD mice with less than the maximum DCX^{+} cell count seen in 5×FAD^{CTL} mice were designated "5×FAD$^{\AHN(RUN)}$" mice. Mice were sacrificed at the age of 6–6.5 months, when untreated 5×FAD mice showed cognitive deficits compared to non-transgenic wild-type mice (WT) mice (fig. S1). Endogenous neurogenic changes and AD pathologies observed in untreated 5×FAD mice, including our rationale for employing this mouse line, are described in fig. S2–S3 and Materials and Methods.

We tested whether AHN stimulation by exercise versus P7C3 and LV-Wnt3 affected AE plaque levels. Immunostaining with anti-Aβ antibody 3D6 showed that, while exercised mice exhibited a decreased Aβ burden, activation of AHN alone (by P7C3 and LV-Wnt3) did not change Aβ plaque levels (Fig. 1, C and E). 5×FAD$^{\Psi AHN(RUN)}$ mice also had a reduced Aβ burden, suggesting that an effect due to exercise and not AHN alone contributed to changes in Aβ burden following physical activity.

Increasing AHN alone did not ameliorate cognitive function in 5×FAD mice

We examined whether promoting AHN could ameliorate cognitive impairment in AD. We performed a delayed non-matching to place (DNMP) task to measure spatial pattern separation, an 8-arm radial arm maze (RAM) to measure reference and retention memory, and a Y-maze to measure spatial working memory. Pattern separation, which is the formation of distinct representations of similar inputs, has been shown to require adult-generated neurons (16). Reduced ability to separate patterns (i.e., to recognize differences between very similar events) is one of the first behavioral deficits in patients with mild cognitive impairments, which often progress to AD (17). The other cognition types listed are well accepted to be hippocampus dependent; however, it remains unclear whether AHN contributes to these memory types. We employed the RAM and Y-maze, which are routine methods to assess memory function in AD mice (18), to explore whether increasing AHN also ameliorates AD-associated cognitive impairment in 5×FAD mice.

In the DNMP task, male cohorts of 5×FAD^{ProAHN} and 5×FAD$^{+AHN(RUN)}$ mice showed similar improvements in pattern separation compared to 5×FAD^{CTL} mice at 5.5–6 months of age (Fig. 2A, left graph). However, in female cohorts, 5×FAD^{ProAHN} mice failed to show improved pattern separation memory compared to 5×FAD^{CTL} mice, whereas 5×FAD $^{+AHN(RUN)}$ mice showed improvement (Fig. 2A, right graph). Both male and female 5×FAD^{ProAHN} mice failed to show improved working memory in the Y-maze, whereas 5×FAD$^{+AHN(RUN)}$ mice performed better (Fig. 2B, fig. S4). Male mice were tested in the RAM task. In the training trials of the task, all the groups showed a clear learning curve during the 5-day training session (Fig. 2C, left graph). However, while 5×FAD$^{+AHN(RUN)}$ mice showed significant improved reference memory compared to 5×FAD^{CTL} mice on days 2 and 3, 5×FAD^{ProAHN} mice failed to show improved memory. The performance of

5×FAD^{ProAHN} mice did not differ from 5×FAD^{CTL} mice. In the retention memory task, on day 8, 5×FAD^{ProAHN} mice again failed to show improved memory, whereas 5×FAD $^{+AHN(RUN)}$ mice did (Fig. 2C, right graph). Our results suggest that increasing AHN alone was sufficient to improve pattern separation memory in male 5×FAD mice but not in female mice; however, it was not sufficient to improve other forms of cognition. In contrast, exercise led to improved cognitive function in all 3 types of memory tests.

Interestingly, exercise alone, in the absence of increased AHN, exerted no observed beneficial effects on cognitive function (5×FAD$^{\Psi AHN(RUN)}$, Fig. 2). This finding suggests that increased AHN above physiological levels is required for the positive behavioral effects of exercise in 5×FAD mice. However, a lack of AHN in WT mice does not block the beneficial behavioral effects of increased physical activity gained through living in an enriched environment (19). We hypothesized that adult-generated neurons have unique functions in AD pathological conditions and in mediating the effects of exercise in AD. To test these points, we assessed the effects of AHN ablation in 5×FAD mice versus WT mice.

Ablating AHN induced cell death in dentate gyrus (DG) of 5×FAD mice

To block AHN, 6- to 8-week-old male WT and 5×FAD mice received either focal irradiation (20) (IR; WT^{IR}; 5×FAD^{IR}), the DNA-alkylating agent temozolomide (21) (TMZ; WT^{TMZ}; 5×FAD^{TMZ}), or a lentivirus expressing a dominant-negative form of Wnt (15) (LV-dnWnt; WT$^{LV\text{-}dnWnt}$; 5×FAD$^{LV\text{-}dnWnt}$) (Fig. 3, A to C). They were then sacrificed at 3 or 5 months of age. Sham mice (WT^{Sham}; 5×FAD^{Sham}) and mice treated with vehicle (WT^{Veh}; 5×FAD^{Veh}) or LV-GFP (WT$^{LV\text{-}GFP}$; 5×FAD$^{LV\text{-}GFP}$) served as controls for mice treated with IR, TMZ, and LV-dnWnt, respectively. IR almost completely eliminated AHN, as determined by immunostaining for DCX^{+} neurons, in both WT and 5×FAD mice. Injection of TMZ or LV-dnWnt also showed significant, although variable, AHN knockdown (Fig. 3C; see Table S2 for animal numbers in each experimental group and group arrangement explanations).

To test whether adult-generated neurons are required to maintain stability in existing neuronal populations in AD, we stained brain sections from each group with an antibody against activated Caspase 3 (Casp3), a marker for apoptotic cells, and examined them for evidence of cell loss. 5×FAD^{Sham}, 5×FAD^{Veh}, and 5×FAD$^{LV\text{-}GFP}$ mice showed only a few Casp3^{+} cells in the DG at 5 months of age. Conversely, the number of Casp3^{+} cells was significantly increased in the DG of 5-month-old 5×FAD^{IR}, 5×FAD^{TMZ}, and 5×FAD$^{LV\text{-}dnWnt}$ mice; no such cell death was observed in the corresponding WT treatment groups (Fig. 3, D and E). However, 5×FAD^{TMZ} and 5×FAD$^{LV\text{-}dnWnt}$ mice that showed less than approximately 60% AHN reduction did not exhibit a significant increase in the number of Casp3^{+} cells compared to 5×FAD^{Veh} and 5×FAD$^{LV\text{-}GFP}$ mice, respectively (Fig. 3F). These results suggest that the existence of Casp3^{+} cells in 5×FAD^{TMZ} and 5×FAD$^{LV\text{-}dnWnt}$ mice could be dependent on the degree of AHN knockdown.

Therefore, we regrouped 5×FAD^{TMZ} mice based on the degree of AHN knockdown. 5×FAD$^{TMZ\ (Mod\ KD)}$ showed moderate (less than 60% AHN reduction) and 5×FAD$^{TMZ\ (high\ KD)}$ showed high (over 60% AHN reduction) AHN knockdown. Likewise, the 5×FAD$^{LV\text{-}dnWnt}$ group was regrouped into 5×FAD$^{LV\text{-}dnWnt\ (Mod\ KD)}$ and

5×FAD$^{\text{LV-dnWnt (high KD)}}$ mice. WT mice injected with TMZ or LV-dnWnt were also regrouped into WT$^{\text{TMZ (Mod KD)}}$ and WT$^{\text{TMZ (high KD)}}$ groups, and WT$^{\text{LV-dnWnt (Mod KD)}}$ and WT$^{\text{LV-dnWnt (high KD)}}$ groups. As shown in Fig. 3F, 5×FAD$^{\text{TMZ (high KD)}}$ mice showed significantly increased Casp3^{+} cell numbers compared to both 5×FAD$^{\text{Veh}}$ and 5×FAD$^{\text{TMZ}}$ (Mod KD) mice, whereas 5×FAD$^{\text{TMZ (Mod KD)}}$ mice did not show increased Casp3^{+} cells compared to 5×FAD$^{\text{Veh}}$ mice. Similarly, 5×FAD$^{\text{LV-dnWnt (high KD)}}$ mice showed increased Casp3^{+} cell numbers compared to both 5×FAD$^{\text{LV-GFP}}$ and 5×FAD$^{\text{LV-dnWnt (Mod KD)}}$ mice, whereas no significant difference was observed between 5×FAD$^{\text{LV-GFP}}$ and 5×FAD$^{\text{LV-dnWnt (Mod KD)}}$ mice.

From here on, 5×FAD$^{\text{Sham}}$, 5×FAD$^{\text{Veh}}$, and 5×FAD$^{\text{LV-GFP}}$ mice are collectively referred to as 5×FAD$^{\text{CTL}}$; 5×FAD$^{\text{IR}}$, 5×FAD$^{\text{TMZ}}$, and 5×FAD$^{\text{LV-dnWnt}}$ mice as 5×FAD$^{-\text{AHN}}$ mice; 5×FAD$^{\text{IR}}$, 5×FAD$^{\text{TMZ (High KD)}}$, and 5×FAD$^{\text{LV-dnWnt (High KD)}}$ mice as 5×FAD$^{-\text{AHN (High KD)}}$ mice; 5×FAD$^{\text{TMZ (Mod}}$ KD) and 5×FAD$^{\text{LV-dnWnt (Mod KD)}}$ mice as 5×FAD$^{-\text{AHN (Mod KD)}}$ mice. Likewise, the corresponding groups of WT mice are referred to as WT$^{\text{CTL}}$, WT$^{-\text{AHN}}$, WT$^{-\text{AHN (High KD)}}$ and WT$^{-\text{AHN (Mod KD)}}$ mice, respectively.

Most Casp3^{+} cells were co-labeled with NeuN, a mature neuronal marker (Fig. 4A), suggesting that AHN suppression caused the death of mature neurons. The total number of granule cells was decreased by the death of mature neurons in the 5×FAD$^{-\text{AHN (High KD)}}$ group but not in the WT$^{-\text{AHN (High KD)}}$ group (Fig. 4B), demonstrating the importance of AHN in the survival of the pre-existing granule cell population. The number of granule cells was not decreased in 5×FAD$^{-\text{AHN (Mod KD)}}$ mice. Our results suggest that AHN plays a potential function in maintaining the structural integrity of the DG uniquely under pathological conditions of AD but not under normal physiological conditions.

ELISA and immunoblot assays revealed that the levels of post-synaptic density 95 (PSD95) and synapse-associated protein 97 (SAP97) in the hippocampal homogenates of 5×FAD$^{-\text{AHN (High KD)}}$ mice were reduced compared to 5×FAD$^{\text{CTL}}$ mice at 5 months of age (Fig. 4C, fig. S5). Meanwhile, AHN reduction did not change the levels of PSD95 and SAP97 in WT mice. These results demonstrate that suppressing AHN resulted in considerable loss of synaptic proteins PSD95 and SAP97 in the hippocampus of 5×FAD mice, likely due to DG neuronal cell death.

Golgi staining showed that the morphology of granule neurons in the outer granule cell layer, generated during early development, of 5×FAD$^{\text{IR}}$ mice did not differ from that of neurons of 5×FAD$^{\text{Sham}}$ mice (Fig. 4D, fig. S6). Furthermore, Casp3^{+} cell number did not increase in 5×FAD$^{-\text{AHN (Mod KD)}}$ mice (Fig. 3F). These results suggest that the increase in Casp3^{+} cells and loss of granule neurons and synaptic markers in 5×FAD$^{-\text{AHN (High KD)}}$ mice can be attributed mostly to AHN loss, rather than the direct impact of IR, TMZ, or LV-dnWnt on the existing neurons in the more susceptible brain environment of 5×FAD mice.

Five-month-old 5×FAD mice in which AHN was suppressed much later (at 4–4.5 months) and which had AHN levels similar to untreated 5×FAD mice before AHN was suppressed, exhibited only negligible Casp3^{+} cell numbers (fig. S7A). We also could not detect any significant Casp3^{+} cells in 3-month-old 5×FAD mice in which AHN was ablated starting at

1.5–2 months old (fig. S7B). These results indicate that adult-generated neurons at a relatively early stage of AD (6 weeks to 4 months old) are critical for later maintaining the survival and stability of granule neurons (at 5 months and older). Thus, AHN impairment at a very early disease stage appears to initiate cell death in later stages, i.e., when the neuronal milieu becomes more hostile [e.g., elevated levels of Aβ pathology, interleukin-1β (IL-1β), tumor necrosis factor D (TNFα), and Keratinocyte-derived chemokine (KC/GRO); reduced levels of brain-derived neurotrophic factor (BDNF); fig. S2 to S3]. Blocking AHN did not affect the levels of AE deposition, numbers of $Iba1^{+}$ microglia, or $GFAP^{+}$ astrocytes in the hippocampus of 5-month-old 5×FAD mice (fig. S8), suggesting that AHN in 5×FAD mice had no effect on AE pathology or gliosis.

Ablating AHN exacerbated cognitive impairment in 5×FAD mice

We next investigated whether cognitive dysfunction progressed more rapidly in the absence of AHN in 5×FAD mice. Untreated 5×FAD mice showed significant impairment in pattern separation at 5 months compared to age-matched WT mice, but not at 3 months of age (fig. S1). Therefore, the impact of AHN loss on pattern separation memory was studied in WT^{-AHN} and $5\times FAD^{-AHN}$ mice at 3 months of age. In the DNMP task, both 3-month-old WT^{-AHN} and $5\times FAD^{-AHN}$ mice exhibited equally poor performances; no further impairment was observed in the $5\times FAD^{-AHN}$ mice compared to WT^{-AHN} mice (fig. S9). These results suggest that adult-generated neurons are required for pattern separation both in WT and 5×FAD mice. Thus, decreased AHN in AD is sufficient to cause impairment of this memory type, and other AD pathological factors are not required for this behavioral change.

In the RAM task, 5-month-old WT^{-AHN} mice did not perform differently from WT^{CTL} mice, indicating that WT mice lacking AHN were still capable of performing this task at a normal rate. However, ablating AHN in 5-month-old 5×FAD mice resulted in significant cognitive impairments (Fig. 4E, see Table S3 for statistical analysis and group performance). However, $5\times FAD^{-AHN\ (Mod\ KD)}$ mice performed comparably with $5\times FAD^{CTL}$ mice (Fig. 4F. see Table S4 for statistical analysis and group performance). These results suggest that a high degree of AHN knockdown, accompanied by loss of granule cells and synaptic markers, exacerbates AD-associated cognitive impairment in 5×FAD mice. Similar results were observed in the Y-maze task except that $5\times FAD^{LV\text{-}dnWnt\ (Mod\ KD)}$ mice also showed impaired memory compared to $5\times FAD^{LV\text{-}GFP}$ mice (fig. S10).

Five-month-old 5×FAD mice in which AHN was ablated starting at 4–4.5 months of age performed comparably to $5\times FAD^{CTL}$ mice in the RAM task (fig. S11). No impairment was observed in 3-month-old $5\times FAD^{-AHN}$ mice in which AHN was suppressed beginning at 1.5–2 months of age compared to those with AHN (fig. S12). These results suggest that loss of AHN, alone, is not sufficient to cause global hippocampal cognitive deficits in 5×FAD mice, and that loss of mature granule neurons (owing to AHN loss at a much earlier age) is minimally required to result in global cognitive deficits later in life (beginning at 5 months of age).

Ablating AHN in male 5×FAD mice reduces hippocampal levels of TGF-β1

The mechanisms by which the lack of AHN contributes to cell death in mature neural populations in 5×FAD mice are likely diverse with multiple pathways, and future efforts will be necessary to elucidate them. Interestingly, among the cytokines we measured, transforming growth factor-E1 (TGF-β1) levels were significantly reduced in the hippocampal tissue homogenates of $5\times FAD^{-AHN\ (High\ KD)}$ mice compared to $5\times FAD^{CTL}$ mice (Fig. 5A, Table S5). TGF-β1 levels were not reduced in $WT^{-AHN\ (High\ KD)}$ mice compared to WT^{CTL} mice (fig. S13), suggesting that AHN loss, accompanied by loss of granule cells and synaptic markers, results in the reduced TGF-E1 levels. TGF-β1 is an anti-inflammatory cytokine that increases rapidly after injury and with age (22). Neurons and multipotent NPCs produce TGF-β1 (23, 24), and TGF-β1 inhibits Casp3 (25). We asked whether TGF-β1 has protective effects against cell death in AD, i.e., whether reduced TGF-E1 levels in $5\times FAD^{-AHN}$ contribute to cell death. For this purpose, we increased TGF-β1 in $5\times FAD^{-AHN}$ mice by injecting lentivirus expressing TGF-β1 (LV-TGF-β1; $5\times FAD^{IR/LV\text{-}TGF\text{-}\beta1}$, $5\times FAD^{TMZ/LV\text{-}TGF\text{-}\beta1}$, and $5\times FAD^{LV\text{-}dnWnt/LV\text{-}TGF\text{-}\beta1}$) and quantified $Casp3^+$ cells (Fig. 5, B to D). These mice experienced increased hippocampal TGF-β1 levels and decreased numbers of $Casp3^+$ cells in the DG compared to 5×FAD mice without AHN injected with control LV-RFP ($5\times FAD^{IR/LV\text{-}RFP}$, $5\times FAD^{TMZ/LV\text{-}RFP}$, and $5\times FAD^{LV\text{-}dnWnt/LV\text{-}RFP}$). However, $Casp3^+$ cells were still evident in the $5\times FAD^{-AHN}$ mice injected with LV-TGF-β1, and increasing TGF-β1 levels was not sufficient to rescue cell death fully in 5×FAD mice without AHN. Our results suggest that TGF-β1 has protective effects against cell death in 5×FAD mice and that the reduced TGF-β1 levels in 5×FAD mice without AHN, at least in part, contribute to granule cell death. Other mechanisms that maintain existing neuronal stability in AD likely account for the fraction of cell death that was not rescued by TGF-β1. Increasing TGF-β1 in $5\times FAD^{-AHN}$ mice did not change the degree of AHN (fig. S14), although TGF-β1 has been shown to regulate neurogenesis (26–29).

Protective effects of TGF-β1 against cell death were confirmed in 3-dimensional (3D) cultures of differentiated human NPCs expressing familial AD-related mutations (3D-FAD cells) (30). Our 3D-FAD cells showed an increased number of $Casp3^+$ cells and endogenous neuronal loss, as indicated by cell counting, compared to control WT cells (3D-WT cells) beginning at 5 weeks of differentiation (fig. S15). Six-week differentiated 3D-FAD cells were treated with TGF-β1 for up to 2 weeks, after which cell viability was assessed. $Casp3^+$ cell number was significantly reduced in 3D-FAD cells treated with TGF-β1 (10 ng/ml; Fig. 5, E and F). Treatment of TGF-β1 significantly increased cell survival in 3D-FAD cells, as indicated by cell counting (Fig. 5, G and H). Furthermore, a lactate dehydrogenase (LDH) assay showed that treatment with TGF-β1 resulted in decreased LDH release (fig. S16A). Protective effects of TGF-β1 were also shown by a CellTiter-Glo luminescent assay, in which cell viability was increase with TGF-β1 treatment (fig. S16B).

Endogenous levels of TGF-β1 were measured in 0.5-, 5-, and 8-week differentiated 3DWT and 3D-FAD cultures (fig. S17A). Considering that our 3D cultures are composed of mostly neurons, with astrocyte presence, and do not contain microglia, the endogenous TGF-β1 detected in our 3D culture models was secreted from neurons and/or astrocytes. At 0.5 week

of differentiation, TGF-β1 levels were higher in the 3D-FAD cultures compared to 3D-WT. While TGF-β1 levels in the 3D-WT did not differ significantly at the three time points, in the 3D-FAD culture, levels of TGF-β1 were significantly reduced in the 5- and 8-week differentiated cultures, where cell death occurred, compared to the 0.5-week differentiated cultures. When normalized by actin signal density, TGF-β1 levels in the 5- and 8-week differentiated 3D-FAD cultures did not differ from those in age-matched 3D-WT cultures (fig. S17B), suggesting that the decrease in TGF-E1 observed in 3D-FAD cultures compared to 3D-WT cultures was due to cell loss. However, we also observed that TGF-β1 levels normalized by actin signal were significantly lower in the 8-week differentiated 3D-FAD cultures compared to 5 week-differentiated 3D-FAD cultures. Therefore, we cannot exclude the possibility that the reduced levels observed at the 8-week time point were also attributable to specific signaling inhibitions.

Effects of ablating AHN in female 5×FAD mice

AHN loss in female 5×FAD mice was accompanied by an increased $Casp3^+$ cells in the DG, reduced hippocampal levels of PSD95, and exacerbated cognitive dysfunction (Fig. 6, A to E, fig. S18; see fig. S18A for animal number in each experimental group and group arrangement explanations). However, these mice did not show reduced hippocampal levels of TGF-β1 (Fig. 6F). Thus, we measured endogenous levels of TGF-β1 in the hippocampus of untreated male and female WT and 5×FAD mice at different ages (Fig. 6G). Untreated female 5×FAD mice showed significantly increased TGF-β1 levels as compared to WT mice and increased, although not statistically significant, TGF-β1 levels as compared to male 5×FAD mice at 5 months of age. The relatively increased levels of TGF-β1 in female 5×FAD mice might mask the ability to observe a small reduction of TGF-β1, as observed in male 5×FAD mice without AHN. Therefore, blocking AHN might result in reduction of TGF-β1 in 5×FAD mice at an age when endogenous TGF-β1 levels are not yet increased as compared to WT mice. AHN loss still increased $Casp3^+$ cell numbers in female 5×FAD mice, suggesting that reduction of TGF-β1 is most likely not the only mechanism underlying cell death in 5×FAD mice lacking AHN.

Exercise increased levels of hippocampal BDNF, PSD95, SYP, IL-6, and FNDC5.

We addressed the mechanism by which the combination of exercise and increased AHN, but not increased AHN alone, improved cognition in the 5×FAD mice. Exercise has been shown to increase neurotrophins, growth factors, and synaptic markers, and to reduce neuroinflammation (31–35). Exercise induces fibronectin type III domain-containing protein-5 (FNDC5) that regulates hippocampal BDNF expression in mice (36). We first measured 18 molecules in the hippocampus of untreated sedentary and exercised 5×FAD mice, and found that exercise increased the levels of hippocampal BDNF, PSD95, synaptophysin (SYP), interleukin-6 (IL-6), and FNDC5 (Table S6). We next measured the levels of these molecules in the $5\times FAD^{CTL}$, $5\times FAD^{ProAHN}$, $5\times FAD^{+AHN(RUN)}$, and $5\times FAD^{\Psi AHN(RUN)}$ mice. Exercise again led to increased levels of hippocampal BDNF, PSD95, SYP, IL-6, and only in male mice, FNDC5, whereas activating AHN alone did not

(Table 1 and S7). Considering that AD patients have reduced levels of BDNF, PSD95, and SYP (37–39) and that these proteins are important regulators of synaptic plasticity, the increase in these protein levels with exercise combined with increased AHN may contribute to an improved behavioral outcome for patients, as observed in the 5×FAD$^{+AHN(RUN)}$ mice. IL-6, for which levels are selectively elevated in the hippocampus following exercise (40), has also been reported to benefit cognition and regulate neurogenesis (41–45).

AHN activation combined with increased BDNF levels genetically ameliorates cognitive function in 5×FAD mice

To explore the mechanisms underlying cognitive improvement after combined exercise and increased AHN, we directly increased BDNF, IL-6, or FNDC5 in the hippocampus of 5×FAD^{ProAHN} mice. We investigated whether increasing levels of these factors in conjunction with increased AHN would result in cognitive improvements mimicking those observed in the 5×FAD$^{+AHN(RUN)}$ mice. To increase BDNF in the 5×FAD^{ProAHN} mice, lentivirus expressing BDNF (LV-BDNF) was injected in the hippocampus at 3 months of age when they received LV-Wnt3 (5×FAD$^{ProAHN/LV-BDNF}$; Fig. 7A). Lentivirus expressing red fluorescent protein (LV-RFP) was injected into additional 5×FAD^{ProAHN} and 5×FAD$^{+AHN(RUN)}$ mice (5×FAD$^{ProAHN/LV-RFP}$ and 5×FAD$^{+AHN(RUN)/LV-RFP}$ mice, respectively). LV-BDNF injection increased hippocampal BDNF levels in both 6-month-old male and female 5×FAD^{ProAHN} mice (Fig. 7B, see Table S8 for statistical analysis of Fig. 7 experiments). Although BDNF has been shown to regulate AHN positively (46), LV-BDNF injection did not further increase the number of DCX^{+} neurons in 5×FAD mice treated with P7C3 and LV-Wnt3, and the number of DCX^{+} neurons was comparable in all groups (Fig. 7C). LV-BDNF injection did not affect Aβ plaque levels (Fig. 7D).

In the Y-maze, both male and female 5×FAD$^{+AHN(RUN)/LV-RFP}$ mice showed improved memory compared to the 5×FAD$^{ProAHN/LV-RFP}$ mice of both genders (Fig. 7E, fig. S19). 5×FAD$^{ProAHN/LV-BDNF}$ mice also exhibited similar memory improvement. In male cohorts, during the RAM task training trials, 5×FAD$^{+AHN(RUN)/LV-RFP}$ mice showed improved memory compared to 5×FAD$^{ProAHN/LV-RFP}$ mice (Fig. 7F left graph). Although 5×FAD$^{ProAHN/LV-BDNF}$ mice did not show significant improvement, their performance did not differ from that of either 5×FAD$^{ProAHN/LV-RFP}$ or 5×FAD$^{+AHN(RUN)/LV-RFP}$ mice. However, in the memory retention test, 5×FAD$^{ProAHN/LV-BDNF}$ mice showed memory improvement compared to 5×FAD$^{ProAHN/LV-RFP}$ mice and behaved similarly to 5×FAD$^{+AHN(RUN)/LV-RFP}$ mice (Fig. 7F right graph). Increasing AHN alone by P7C3 and LV-Wnt3 did not improve pattern separation memory in female 5×FAD mice (Fig. 2A right graph). However, increasing AHN in conjunction with BDNF in female 5×FAD mice (female 5×FAD$^{ProAHN/LV-BDNF}$ mice) produced significantly improved pattern separation memory (Fig. 7G).

Increasing BDNF alone, in the absence of promoting AHN by P7C3 and LV-Wnt3, failed to increase AHN or improve memory in 5×FAD mice (Fig. 7, H and I, fig. S20). These results suggest that increasing hippocampal BDNF, in combination with AHN activation, is

sufficient to mimic the beneficial effects of exercise on cognition in 5×FAD mice, even in the continued presence of Aβ plaques.

AHN activation combined with increased BDNF levels pharmacologically ameliorates cognitive function in 5×FAD mice

We next explored whether a late-stage increase in BDNF pharmacologically (AICAR), with increased AHN by P7C3 and LV-Wnt3, could also provide an effective therapeutic strategy comparable to that of sustained exercise in 5×FAD mice. For this purpose, we used the AMP-activated protein kinase agonist 5-aminoimidazole-4-carboxamide riboside (AICAR), which increases BDNF in mice (47). Male and female $5\times FAD^{ProAHN}$ mice were injected with AICAR or saline every other day for 2 weeks starting at 5.5 months of age; they were sacrificed at 6 months of age ($5\times FAD^{ProAHN/AICAR}$ and $5\times FAD^{ProAHN/Veh}$ mice, respectively). Hippocampal BDNF levels were increased in the male and female $5\times FAD^{ProAHN/AICAR}$ mice compared to $5\times FAD^{ProAHN/Veh}$ mice, and their levels were not different from those of $5\times FAD^{+AHN(RUN)}$ mice injected with saline ($5\times FAD^{+AHN(RUN)/Veh}$; Fig. 7J). The number of DCX^{+} neurons was comparable among all groups (fig. S21A).

Male mice were tested in the Y-maze and RAM tasks, and female mice were tested in the Y-maze and DNMP tasks. In the Y-maze, $5\times FAD^{ProAHN/AICAR}$ mice showed improved memory compared to the $5\times FAD^{ProAHN/LV\text{-}RFP}$ mice in each respective gender, and their performance did not differ from $5\times FAD^{+AHN(RUN)/Veh}$ mice (Fig. 7K, fig. S21B). While male $5\times FAD^{ProAHN/AICAR}$ mice did not perform better than $5\times FAD^{ProAHN/Veh}$ mice in RAM task training trials (fig. S21C), they showed better cognition in the retention test of the task, performing similarly to $5\times FAD^{+AHN(RUN)/Veh}$ mice (Fig. 7L). Female $5\times FAD^{ProAHN/AICAR}$ mice showed improved pattern separation in the DNMP task, performing again similarly to $5\times FAD^{+AHN(RUN)/Veh}$ mice (Fig. 7M).

It has been reported that AICAR alone increases AHN and cognition in WT mice (47, 48). However, AICAR alone failed to increase AHN in the 5×FAD mice, although it increased hippocampal BDNF levels (fig. S22A). No effect of AICAR was observed in the cognition tasks that we employed in 5×FAD mice with no AHN activation (fig. S22B-S22D). These results suggest that a late-stage increase in BDNF by AICAR, in the presence of promoted AHN, was also able to mimic the beneficial effects of exercise on cognition in 5×FAD mice.

Future studies will be needed to explore the mechanisms by which increasing levels of BDNF and AHN combine to mimic the benefits of exercise on cognition in AD. LV-BDNF injection increased levels of hippocampal PSD95, whereas AICAR did not (Table S9). Neither LV-BDNF nor AICAR increased IL-6 levels (Table S9). These results suggest that the beneficial effects of increasing both AHN and BDNF on cognition could be independent of PSD95 or IL-6. Directly increasing levels of hippocampal IL-6 or FNDC5 via lentivirus failed to improve cognition or increase BDNF in $5\times FAD^{ProAHN}$ mice. However, it is possible that only the secreted form of peripherally expressed FNDC5 is responsible for exercise-induced hippocampal BDNF, as peripheral delivery of FNDC5 induces the expression of hippocampal BDNF (36). To note, there may be other possible effects of AICAR aside from increasing BDNF levels. TGF-β1 levels were not changed by increasing

AHN with or without increased BDNF, increasing BDNF only, or by exercise in our study (Table S10).

Discussion

In the present study, we did not explore the effects of AHN manipulation on tau phosphorylation levels since basal tau phosphorylation is already present in adult-generated neurons at DCX^+ immature neuronal stages [(49), see fig. S23]. Future studies are necessary to investigate whether adult-generated neurons affect tauopathy in the human AD brain. The effects of physical exercise on cognition in patients with dementia are inconclusive (50–52). In our study, $5\times FAD^{\Psi AHN(RUN)}$ mice did not show improved cognitive function, suggesting that increased AHN is required to mediate the beneficial effects of exercise in 5×FAD mice. Individuals who remain cognitively intact despite showing neuropathological AD features have increased number of neural stem cells compared to AD subjects (53). Therefore, future studies are required regarding whether patients with dementia who experienced physical exercise have increased AHN enough to have beneficial effects of exercise on cognition.

In summary, inducing AHN alone, e.g., pharmacologically and genetically, conferred only minimal to no benefit in 5×FAD mice. However, exercise-induced AHN improved cognition along with reduced Aβ load and increased levels of BDNF, IL-6, FNDC5, and synaptic markers. AHN activation was also required for exercise-induced improvement in memory. These data suggest that promoting AHN can ameliorate AD pathology and cognitive deficits but only in the presence of a healthier, improved local brain environment, e.g., stimulated by physical exercise. Interestingly, increasing AHN alone (genetically and pharmacologically) combined with overexpression of BDNF was able to mimic exercise-induced improvements in cognition, without reducing Aβ burden. We also found that deficits in AHN in very early stages of life can exacerbate neuronal vulnerability in AD later in life, leading to cognitive impairment and increased neuronal loss, due at least in part to reduced TGF-β1. These results suggest that adult-born neurons generated very early in life are critical for maintaining hippocampal neuronal populations in the abnormal and hostile brain environment created by AD later in life. Thus, AHN impairment may be a primary event that later mediates other aspects of AD pathogenesis. Future attempts to create pharmacological mimetics of the benefits of exercise on both increased AHN and the health of the local neuronal environment, especially involving increased BDNF levels, may someday provide an effective means for improving cognition in AD. Moreover, increasing neurogenesis in the earliest stages of AD pathogenesis may protect against neuronal cell death later in the disease, providing a potentially powerful disease-modifying treatment strategy for AD.

Materials and Methods

Animals

We used 5×FAD APP/PS1 doubly transgenic mice that co-overexpress and co-inherit FAD mutant forms of human amyloid precursor protein (APP) (the Swedish mutation: K670N, M671L; the Florida mutation: I716V; the London mutation: V717I) and presenilin 1 (PS1) (M146L; L286V) transgenes under transcriptional control of the neuron-specific mouse Thy-1 promoter (Tg6799 line). 5×FAD lines (B6/SJL genetic background) were purchased

from Jackson Laboratory and were maintained by crossing heterozygous transgenic mice with B6/SJL F1 breeders. All 5×FAD transgenic mice were heterozygotes with respect to the transgene. Animal experiments were conducted in accordance with institutional and NIH guidelines.

Observed benefits of employing the 5×FAD mouse model

Most of the current AD transgenic mouse models are generated by the overexpression of mutation(s) related to familial AD (FAD). While the 5×FAD mouse model expresses rare early-onset FAD mutations, the pathological features found in the brains of 5×FAD mice are common to all forms of AD. In the current study, we examined the manner in which altered AHN affects cell survival and cognition under these pathological conditions. Hence, we believe that the results of our experiments are also relevant for generalized AD pathology (beyond that of early-onset FAD).

We chose 5×FAD mice, which show faster AD progression compared to other AD transgenic mice, based on our goal of investigating whether impaired AHN at an early stage in AD resulted in neuronal/synaptic loss and in accelerated cognitive impairment at later stages of the disease. We also aimed to investigate whether adult-generated neurons affected the preexisting neuronal populations and whether impaired AHN exacerbated neuronal loss in AD.

5×FAD mice are one of the few AD transgenic mouse models that exhibit neurodegeneration, thus rationalizing our use of this model. In addition, performing long-term manipulations of AHN is challenging and can compromise the health of mice over time. For example, multiple irradiations cause neuro-inflammation. Long-term injections of TMZ cause side effects, including weight loss and hair loss (personal observations). Lentivirus is delivered to the brain using stereotaxic surgery, and multiple brain surgeries are not possible. Thus, studying the 5×FAD line, which undergoes more rapid AD progression compared to other AD transgenic mice, is advantageous for our study.

Generation of LV-Wnt3 and LV-dnWnt

To construct the Wnt3-Internal ribosomal entry site (IRES)-GFP vector, we cloned the cDNA of Wnt3 upstream of the IRES and GFP and inserted the bicistronic cassette in place of the GFP sequence in the pRRL.SIN.cPPT.hPGK.GFP.Wpre vector. To generate the dnWnt-IRES-GFP vector, we cloned the cDNA for dnWnt upstream of the IRES and GFP and inserted the bicistronic cassette in place of the GFP sequence in the CSC.cPPT.hCMV.GFP.Wpre vector. Concentrated lentiviral stocks were produced by calcium phosphate transfection into 293T cells. Supernatants were collected, passed through a 0.22-μm filter, and purified by ultracentrifugation. Viral stocks were stored at −80°C until use and were diluted at 0.8×10^9 - 1×10^9 transducing units/ml.

Treatment of aminopropyl carbazole (P7C3) and LV-Wnt3, and exercise setting

To increase neurogenesis, 2-month-old 5×FAD mice received 20 mg/kg of P7C3 (Sigma, St. Louis, MO; Asinex, Winston-Salem, NC) once daily for 4 or 5 days a week intraperitoneally (i.p.) over the span of 4–4.5 months. P7C3 was prepared for dosing by dissolving a

recrystallized stock in DMSO at 50 mg/ml. The compound was diluted to a final formulation of 3% DMSO/10% cremophor EL (Sigma, St. Louis, MO)/87.5% D5W (5% dextrose in water, pH 7.2). At the age of 3 months, these mice also received 4 intrahippocampal injections of 0.5 Pl (total 2.0 Pl) LV-Wnt3 viral suspension at these coordinates: AP, −2.0; ML, ±1.5–1.7; DV, −2.0 and AP, −3.0; ML, ±3.0; DV, −3.0. Injections were performed using a 5 μl Hamilton syringe with a 30-gauge needle attached to a digital stereotaxic apparatus and an infusion pump at a rate of 0.15 μl/min. After virus infusion was completed, the needle remained in place for 10 min before slow withdrawal. The mice were not injected with P7C3 both 3 days prior to and following the LVWnt3 injection day. Control 5×FAD mice received vehicle solution [3% DMSO/10% cremophor EL (Sigma, St. Louis, MO)/ 87.5% D5W (5% dextrose in water, pH 7.2) with no P7C3] and LVGFP.

Both groups were either singly housed either in standard laboratory cages (27 cm × 11 cm × 17 cm) only or singly spent 3 hr in rat cages (45 cm × 20 cm × 20 cm) without running wheels and then were returned to their original cages for 21 hr. A cohort of control 5×FAD mice treated with vehicle and LV-GFP singly spent 3 hr in rat cages equipped with running wheels and was returned to their original cages for the remaining 21 hr, as described previously (11), from between the ages of 6 weeks and 2 months until the end of the experiments.

To evaluate potential changes in neurogenesis, we determined the number of DCX^+ cells in the targeted (GFP-expressing) areas. Areas infected by LVs were identified by expression of GFP.

Blocking AHN

To block AHN, 1.5- to 2-month-old WT and 5×FAD mice received IR, TMZ or LV-dnWnt and were sacrificed at 3 or 5 months of age. Irradiation was not used for mice that were sacrificed at 3 months of age since it requires approximately 1 month of recovery time. Additional 4- to 4.5-month-old 5×FAD mice received TMZ or LV-dnWnt and were sacrificed at 5 months of age.

Irradiation procedure

Mice were anesthetized with ketamine and xylazine, placed in a stereotaxic frame and put into a custom-made radiation shield consisting of a chamber with 1-inch thick lead and a 2.5 mm borehole. The shield covered the entire body but left a 2.5-mm treatment field above the hippocampus. Mice received irradiation once at the dose of 1000 cGy, administered at approximately 90 cGy per minute for a total irradiation time of 11 minutes. A Gammacell 40 Exactor (Theratronics, Ottawa, Ontario) with two Caesium-139 sources was used.

TMZ injection

The DNA-alkylating agent TMZ (Merck & Co., Inc., Whitehouse Station, NJ; Sigma, St. Louis, MO) was dissolved in phosphate buffered saline (PBS) or in dimethyl sulfoxide (DMSO) followed by diluting in PBS to a concentration of 2.5 mg/ml (10% DMSO for TMZ from Sigma). TMZ was administered i.p. at a dose of 12.5 mg/kg once daily for 3 consecutive days, followed by 4 days of no injections (one cycle). After every 4 cycles, mice

were given a 2-week rest period. Vehicle solution was the identical DMSO/PBS solution but without TMZ and was administered in volumes consistent with TMZ dosing.

LV-dnWnt injection

Stereotaxic injections of LV-dnWnt were performed as described above for LV-Wnt3 injections.

Injections of LV-TGF-β1 and LV-BDNF

LV-TGF-β1, LV-BDNF, LV-IL-6, IL-FNDC5, and control LV-RFP were purchased from ViGene Biosciences (Rockville, MD). 5×FAD^{Sham}, 5×FAD^{IR}, 5×FAD^{Veh}, and 5×FAD^{TMZ} mice received 4 intrahippocampal injections of 0.5 Pl (total 2.0 Pl) of LV-TGF-β1 or LV-RFP viral suspension (AP, −2.0; ML, ±1.5–1.7; DV, −2.0 and AP, −3.0; ML, ±3.0; DV, −3.0) at the age of 2.5–3 months. For injections of LV-dnWnt along with LV-TGF-β1 or LV-RFP in 5×FAD mice, 1.5- to 2-month-old mice received 4 intrahippocampal injections of total 2.4–3.0 Pl of LV-dnWnt with LV-TGF-β1 or LV-RFP viral suspension. For injection of LV-BDNF, 5×FAD^{ProAHN} mice received LV-BDNF at the age of 3 months when they received LV-Wnt3: total 2.4–3.0 μl of LV-Wnt3 with LV-BDNF or LV-RFP viral suspension.

Treatment of 5-aminoimidazole-4-carboxamide-1-β-D-ribofuranoside (AICAR)

Mice were injected (i.p.) with AICAR (Toronto Research Chemicals Inc., Canada) dissolved in saline, 250 mg/kg/day, or with saline, every other day for 2 weeks. During the 2 weeks, P7C3 was not injected.

5-Bromo-2'-deoxyuridine (BrdU) injections

BrdU (Sigma, St. Louis, MO) was dissolved in 0.9% NaCl at a concentration of 20 mg/ml and was filtered (0.2 μm) under sterile conditions. Mice received a single i.p. injection of BrdU (50 mg/kg) daily for 3 days and were perfused 1 day after the last BrdU injection and processed for BrdU immunostaining to identify proliferating neural progenitor cells (NPCs). Parallel cohorts of animals from each group were sacrificed 4 weeks after the last BrdU injection and processed to determine the rate of NPC survival and differentiation.

Behavior tests

We performed 3 different behavioral tests: a delayed non-matching to place (DNMP) task to measure pattern separation, an 8-arm radial arm maze (RAM) to measure reference memory and retention memory, and a Y-maze to measure short-term spatial (working) memory. For the DNMP and RAM tasks, mice were food restricted to 90% of their pre-experimental free-feeding weights with water available *ad lib*. We confirmed that our food deprivation regime did not affect AHN in WT and 5×FAD mice. Behavior analyses were performed blindly.

DNMP task

Pattern separation-dependent memory was tested in the DNMP task in the RAM apparatus as described previously (16) with modifications. The testing apparatus was a rat-sized RAM. The maze consisted of 8 equally spaced arms that radiated from an octagonal central platform. Arms were 15 cm wide by 75 cm long, and the walls on each arm were 2.5 cm

high. On the morning before testing commenced, mice were habituated to the maze, where all arms were unblocked and all wells at the end of the arms contained several sunflower seeds. Mice were allowed to explore the maze freely during this habituation session for 30 min. Each trial of this task consisted of a sample phase and a choice phase.

During the sample phase, all arms except a start arm and the sample (rewarded) arm were blocked off. Each mouse was permitted to visit the sample arm and retrieve a food pellet reward. Mice were retrieved from the maze after either (1) spending 10 seconds in the sample arm after retrieving the pellet or (2) exiting the sample arm. During the choice phase, arms in the start and sample (unrewarded) locations and an additional correct (rewarded) location were open. The correct arm was distant from the sample arm by a spatial separation of 2 arms. In this phase, mice were tested for the ability to select, from a choice of 2 arms, the arm location that had not been presented in a previous sample phase. Mice that entered the correct (new, rewarded) arm were considered to have made correct choices. Mice that entered an incorrect (familiar, unrewarded) arm were allowed to self-correct. Mice went through 4 trials (sample plus choice phases) per day for 3 consecutive days.

RAM

The RAM was used for testing spatial reference and retention memory. To adapt to the maze and bait (pretraining), the mice experienced free movement and feeding in a RAM twice a day for 2 days. The bait was scattered in all arms and a sunflower seed in a food cup was available at the end of each arm. The training trial was started following the pretraining. During the training trial, each mouse was given 2 trials daily for 5 days. The same 2 arms were baited each day and across sessions; thus mice learned to ignore the remaining 6 arms that never contained a reward. A trial consisted of placing the mouse in the maze where it remained until both of the 2 reinforcements had been received or until 5 min had elapsed, whichever occurred first. Entry into a never-baited arm was considered a reference memory error, and choices of arms were recorded. Memory retention trial was conducted 3 days after the last training trial in the reference memory test of RAM task.

Y-maze

Short-term spatial memory was assessed by recording spontaneous alternation behavior in a Y-maze, which does not involve any training, reward, or punishment. The ability to alternate requires mice to know which arms have already been visited. Therefore, alternation behavior can be regarded as a measure involving spatial working memory. Each mouse was placed in the center of the symmetrical Y-maze and was allowed to explore freely through the maze during an 8-min session. The sequence and total number of arms entered were recorded. Arm entry was considered to be complete when the hind paws of the mouse had been completely placed in the arm. An alternation was defined as entries into all 3 arms on consecutive occasions. The number of maximum alternation was therefore the total number of arm entries minus 2, and the percentage of alternation was calculated as (actual alternations / maximum alternations) × 100.

Tissue processing

After behavioral tasks, mice were deeply anesthetized with a mixture of ketamine and xylazine and then decapitated. Isolated brains were bisected longitudinally and hemispheres were separated. Hippocampal tissues were dissected from the left hemisphere and frozen on dry ice for biochemical studies. The right hemisphere was kept in 4% paraformaldehyde (PFA) in cold 0.1 M phosphate buffer (pH 7.4) for 3 days, followed by incubation in 30% sucrose solution for immunostaining. Mice injected with BrdU were deeply anesthetized with a mixture of ketamine and xylazine, and perfused transcardially with 4% PFA in cold 0.1 M phosphate buffer (pH 7.4) after 0.9% NaCl. The brains were postfixed overnight and then transferred into a 30% sucrose solution and kept there until they sank. For immunostaining, 40-μm coronal sections were cut from a dry ice-cooled block on a sliding microtome (Leica, Wetzlar, Germany). The sections were stored at −20°C in a cryoprotective buffer containing 28% ethylene glycol, 23% glycol and 0.05 M phosphate buffer until processing for immunohistochemistry or immunofluorescence.

Immunohistochemistry and immunofluorescence confocal microscopy

Immunohistochemistry and immunofluorescent labeling were performed as described previously (54). The antibodies used were rat anti-BrdU (1:100, Accurate Chemical & Scientific Corporation, Westbury, NY), biotin-conjugated mouse anti-BrdU (1:100, Millipore, Temecula, CA), goat anti-DCX (1:200, Santa Cruz Biotechnology, Dallas, Texas), mouse anti-neuronal nuclei (NeuN, 1:500, Chemicon, Temecula, CA), rabbit anti-Fox3/NeuN (1:500, EnCor Biotechnology Inc., Gainesville, FL), rabbit anti-Glial Fibrillary Acidic Protein (GFAP, 1:500, Dako, Fort Collins, CO), rabbit anti-ionized calcium-binding adaptor molecule 1 (Iba1, 1:500, Wako, Osaka, Japan), goat anti-Iba1 (1:500, Abcam, Cambridge, MA), mouse anti-Aβ 3D6 antibodies (1:2,500, a gift from Lilly), and rabbit monoclonal anti-cleaved Caspase 3 (Casp3, 1:1,000, Cell signaling, Danvers, MA).

The immunohistochemical staining was made using the avidin-biotin complex (ABC) system and nickel-enhanced diaminobenzidine (DAB) incubation (Vectastain Elite, Vector labs, Burlingame, CA). Sections were mounted on gelatin-coated slides, air-dried, dehydrated, cleared, and coverslipped. The fluorescent secondary antibodies used for immunofluorescent labeling were donkey anti-goat IgG conjugated with Cy2 or Cy3; donkey anti-rat IgG conjugated with Cy2 or Cy3; donkey anti-mouse IgG conjugated with Cy2 or Cy3 or Cy5; donkey anti-rabbit IgG conjugated with Cy2 or Cy3 or Cy5 (all 1:250, Jackson ImmunoResearch, West Grove, PA). Fluorescent signals were detected using a LSM Pascal 5 Carl Zeiss confocal laser scanning microscope (Zeiss, Germany). Images were captured and recorded using a Zeiss LSM image browser.

For BrdU staining, DNA was denatured by incubating the sections for 2 h in the 50% formamide/2× SSC (0.3 M NaCl and 0.03 M Sodium citrate) at 65°C. Sections were rinsed for 15 min in 2× SSC and incubated for 30 min in 2 N HCl at 37°C. Acid was neutralized by rinsing the sections for 10 min in 0.1 M boric acid (pH 8.5) followed by several washes in Tris-buffered saline (TBS, pH 7.5).

Quantification of immunoreactivity and mouse regrouping

For estimating total $BrdU^+$ cells, a series of systematically selected every sixth brain section was stained, and $BrdU^+$ cells in the subgranular cell layer (SGL) and granular cell layer (GCL) were counted by collecting images under 40× objective on a light microscope (TE360 Eclipse, Nikon, Japan) or a confocal microscope (LSM Pascal 5 Carl Zeiss, Germany). The sum of the $BrdU^+$ cell counts was multiplied by 6 to obtain an estimate of total numbers. For co-labeling analysis of differentiated $BrdU^+$ cell types with lineage-specific markers, the phenotypes of 30 $BrdU^+$ cells per animal were determined. Both the $BrdU^+$ cell count and the phenotype analysis were performed blindly.

For quantification of DCX^+ cells, a series of systematically selected every sixth or twelfth brain section from each mouse was taken from similar regions spanning between bregma −1.34 mm and −3.28 mm using a Mouse Brain Atlas [Paxinos G, Franklin KBJ (2001) The mouse brain in stereotaxic coordinates, Academic Press, San Diego]. The numbers of DCX^+ cells were counted in the inner rim, defined as the border between the hilus and GCL, under 20× objective lens manually. The inner rim length of GCL was measured using a Zeiss LSM image browser (Carl Zeiss, Germany) or Imaris software (Bitplane, Concord, MA). Based on the results of DCX^+ cell numbers, mice were regrouped for additional behavioral data analysis and biochemical/immunostaining experiments. See Table S1, S2, and Fig. S18A for the number of animals in each experimental group and explanations of group arrangement.

For quantification of $Casp3^+$ cells, a series of systematically selected every sixth brain section was stained, and $Casp3^+$ cells in the SGL and GCL were counted by collecting images under 40× objective on a light microscope (TE360 Eclipse, Nikon, Japan) or a confocal microscope (LSM Pascal 5 Carl Zeiss, Germany). The sum of the $Casp3^+$ cell counts was multiplied by 6 to obtain an estimate of total numbers. Researchers who were unaware of the experimental group to which the samples belonged quantified DCX^+ or $Casp3^+$ cells.

Total granule cell counting

Granule cell numbers were determined using unbiased stereologic counting methods. Each sixth section containing the hippocampus was Nissl stained. Optical disector frames (15 × 15 Pm) were set in as systematic-random fashion, accounting for 1% of the area of the GCL on each section. Cells were counted in 5-Pm-thick stacks of optical disectors (1 Pm in depth for each disector), according to stereologic principles. The total number of GCL neurons was obtained by using the formula developed as described previously (55). The granule cell counting was performed blindly.

Quantitative assessment of amyloid deposition

To examine the impact of AHN manipulation or exercise on amyloid deposition, a series of systematically selected (every twelfth) brain sections from each mouse was probed with AE-specific 3D6 antibodies, detected by fluorescently labeled secondary antibodies. Images to quantify the amyloid burden were collected in a Z series of 40-μm depth with 4-μm intervals between images. The volume of amyloid burden was quantified using ImageJ (Voxel counter

plugin), and the area of Aβ immunoreactivity was assessed after adequate thresholding and isolated noise despeckling.

Quantitative cytokine level measurement and ELISAs

Hippocampal tissues were homogenized in RIPA buffer (Sigma, St. Louis, MO) and centrifuged at 45,000 g for 30 min at 4°C. Supernatants were used to measure 10 cytokines: Interleukin 1β (IL-1β), IL-2, IL-4, IL-5, IL-6, IL-10, IL-12p70, Tumor necrosis factor α (TNFα), Interferon γ (IFNγ), and Keratinocyte-derived chemokine (KC/GRO). The measurement of cytokines was performed using the MesoScale Discovery (MSD, Rockville, MD) 96-well Mouse Pro-Inflammatory V-PLEX Assay as outlined in the manufacturer's protocol. Briefly, 25 Pl each of sample and calibrator were added to the plate coated with an array of cytokine capture antibodies. The plate was then incubated for 2 h with vigorous shaking at room temperature, followed by washing with wash buffer (provided in the kit). A volume of 25 Pl of the detection antibody solution was added and incubated for 2 h with vigorous shaking at room temperature. The plate was washed with wash buffer before adding 150 μl 2× MSD Read Buffer, and immediately read on a Meso QuickPlex SQ 120.

For TGF-β1, PSD95, SAP97, SYP, and FNDC5 analyses, supernatant samples were further diluted in cold PBS. For TGF-β1, diluted samples were acidified to pH < 3 with 1N HCl and incubated for 1 h at room temperature, followed by neutralization to pH ~8 with 1N NaOH. Levels of TGF-β1 were measured using TGF-β1 Platinum ELISA kits (Affymetrix eBioscience, San Diego, CA) according to the manufacturer's protocols. PSD95, SAP97, SYP, and FNDC5 contents were measured using ELISA kits from MyBioSource (San Diego, CA) according to the manufacturer's protocols. BDNF protein levels were measured using BDNF ELISA kits (R&D Systems, Minneapolis, MN). TGF-β1 in the media of the 3D cultures were measured using the MSD 96-well TGF-0β1 kit (Rockville, MD).

Immunoblot analysis

15–75 μg of protein were resolved on 12% Bis-Tris or 4–12% gradient Bis/Tris gels (Life Technologies, Grand Island, NY), and the proteins were transferred to the nylon membranes (Bio-Rad, Hercules, CA). Immunoblot images were visualized by enhanced chemiluminescence (ECL). The images were captured by using BioMax film (Kodak, Rochester, NY) or VersaDoc imaging system (Bio-Rad, Hercules, CA) and quantitated by using QuantityOne software (Bio-Rad, Hercules, CA). Primary antibodies were used at the following dilutions: anti-PSD95 (1:500, NeuroMab, Davis, CA), anti-synapse-associated protein 97 (SAP97, 1:500, NeuroMab, Davis, CA), and anti-synaptophysin (SYP, 1:1,000, Millipore, Temecula, CA).

Golgi staining

Golgi staining was performed using the FD Rapid Golgi Stain Kit (FD Neurotechnologies, Inc., Columbia, MD), a simplified and reliable kit for Golgi impregnation, to label neurons in the outer layer of GCLs. Animals were deeply anesthetized with an isoflurane, and the brains were immediately removed and rinsed in MilliQ water. After the rinse, retrieved brains were immersed in a Golgi-Cox solution comprising potassium dichromate, mercuric chloride, and potassium chromate. This mixture of solutions was replaced once after 6 h of

initial immersion, with storage at room temperature in darkness for 2 weeks. After the immersion period in the Golgi-Cox solution, the embedded brains were transferred to a cryoprotectant solution (FD Rapid Golgi Stain Kit) and stored at room temperature for at least 72 hours in the dark before cutting. The brain slices were sectioned in the coronal or sagittal plane at approximately 250 Pm thickness on a cryostat. Sliced tissues were transferred onto gelatin-coated slides and were air dried at room temperature in the dark. After drying, sections were rinsed with distilled water and were subsequently stained in a developing solution (FD Rapid Golgi Stain Kit) and dehydrated with 50%, 75%, 95%, and 100% ethanol. Finally, the sections were defatted in xylene substitute and coverslipped with either Permount (Fisher Scientific, Fair Lawn, NJ).

Images were acquired from prepared slides using a Zeiss 510 microscope. Each neuron was scanned under high (100×, oil immersion) magnification by varying the depth of the Z plane to ensure that all parts of the cell (especially dendrites) were intact. Dendrites that tapered to a point were assumed to be complete and uncut. At least 20 neurons were selected. 3D neuronal reconstruction was performed by LSM510 (Zeiss). The total length and number of branches of dendrites and the spine density were measured by Imaris software (Bitplane, Concord, MA). Seven neurons per mouse were examined.

Treatment of 3D FAD ReN cell cultures with TGF-β1

ReNcell VM human NPCs (ReN cells, EMD Millipore, Billerica, MA) were transfected with internal ribosome entry site (IRES)-mediated polycistronic lentiviral vectors containing FAD genes encoding human APP with both Swedish (K670N/M671L) and London (V717I) mutations, or PS1ΔE9 mutation along with APP Swedish/London mutations, with GFP as a reporter for viral infection. Fluorescence-activated cell sorting (FACS) was then used to enrich the population of cells with the highest expression levels. ReN cells with GFP alone served as controls. The FACS-sorted ReN cells expressing high levels of FAD genes were differentiated and maintained in a 3D Matrigel culture system. Differentiation media containing either 1, 5, or 10 ng/ml of active human TGF-β1 (Abcam, Cambridge, MA) were added to 6-week differentiated cultures every 3 days, and the cells were maintained for an additional 2 weeks. The cell media were collected for Lactate dehydrogenase (LDH) assay, CellTiter-Glo® luminescent cell viability assay and Aβ quantification. The cells were fixed with 4% PFA for Casp3 staining.

LDH assay

CytoTox-ONE assay was performed according to the manufacturer's guidelines (Promega, Madison, WI). 50 μl of cell culture medium was removed from the cells and substrate was added to the cell culture medium in 1:1 dilution and incubated for 30 min in a 37°C incubator. The plate was measured using a spectrophotometer (excitation: 560 nm, emission: 590 nm). Under the influence of the assay's substrate, resazurin is converted to the fluorescent form resorufin due to LDH, which is released into the medium by dead cells only. Therefore, increased values during the experiments were interpreted as increased cell death.

CellTiter-Glo® luminescent cell viability assay

Cell viability was determined using the CellTiter-Glo® luminescent cell viability kit from Promega Corporation (Madison, WI) according to the manufacturer's instructions. This method was based on the measurement of ATP production in the cells, which is proportional to the number of viable cells, detected by luciferin-luciferase reaction. 100 μl of CellTiter-Glo® Reagent was added into the wells. Contents were mixed for 2 min on an orbital shaker to induce cell lysis. The plate was allowed to incubate at room temperature for 10 min to stabilize luminescent signal, and luminescence was recorded.

Casp3 staining using 3D cultures

The fixed cells were permeabilized and blocked by incubating with a blocking solution containing 50 mM Tris (pH 7.4), 0.1% Tween-20, 4% donkey serum, 1% BSA, 0.1% gelatin, and 0.3M glycine at 4°C for 12 h. After washing with TBS buffer containing 0.1% (v/v) Tween-20 (TBST), the 3D cultures were incubated with rabbit monoclonal anti-cleaved Casp3 (1:1,000, Cell signaling, Danvers, MA) antibodies in the blocking solution at 4°C overnight. After washing three times with TBST, the cells were incubated with donkey anti-rabbit IgG conjugated Cy3 for 2 h at room temperature (1:250, Jackson ImmunoResearch, West Grove, PA). To avoid fluorescence quenching, a drop of anti-fade gold (Life Technologies, Grand Island, NY) was added on top of the fixed/stained thin-layer 3D cultures before imaging.

Dot-blot analysis

3D Matrigel samples were dissolved in Lysis Buffer 6 (R&D Systems, Minneapolis, MN) with protease & phosphatase inhibitors (Thermo Scientific, Rockford, IL). One Pl of each sample was spotted onto a LI-COR Biosciences Odyssey Nitrocellulose Membrane (LI-COR Biosciences, Lincoln, NE). The dot blot was then stained for Monoclonal Anti-β-Actin-Peroxidase antibody produced in mouse (Sigma Aldrich, St. Louis, MO) overnight at a dilution ratio of 1:50,000. Then, after sufficient washing the following day, the blot was coated with 2 ml of Pierce ECL Western Blotting Substrate (Thermo Scientific, Rockford, IL). Chemiluminescent detection imaging was then conducted using the Chemi exposure setting on a Li-Cor Odyssey FC machine (LI-COR Biosciences, Lincoln, NE) and then quantified using Image Studio software (LI-COR Biosciences, Lincoln, NE).

Statistical Analysis

Data are expressed as mean values r standard error of the mean (mean ± SEM). Error bars in the figures represent SEM. Differences between groups were analyzed using a *t*-test or an ANOVA that was followed by a post hoc comparison using Tukey or Fisher's LSD, where appropriate. For the RAM tests, a two-way repeated measures analysis of ANOVA was used for main effects (groups) with day as the repeated measure and errors as the dependent variable. In all cases, values of $P < 0.05$ were considered to be significant, and * or # indicated $P < 0.05$ and ** or ## indicated $P < 0.01$. Statistical analysis was performed using PRISM GraphPad statistical software.

Supplementary Material

Refer to Web version on PubMed Central for supplementary material.

Acknowledgments:

Funding: Supported by the Cure Alzheimer's Fund (R.E.T. and S.C.); NIA and NIMH grant 5R01MH060009 (R.E.T.); NIH/NIA grant 1RF1AG048080–01 (R.E.T. and D.K.); NIH/NIA grant 2R01AG014713 (D.K.); the Mather's Foundation, The Leona M. and Harry B. Helmsley Charitable Trust, and the JPB Foundation (F.H.G.).

References and Notes:

1. Tanzi RE, Bertram L, Twenty years of the Alzheimer's disease amyloid hypothesis: a genetic perspective. Cell 120, 545–555 (2005). [PubMed: 15734686]
2. Eriksson PS et al., Neurogenesis in the adult human hippocampus. Nat Med 4, 1313–1317 (1998). [PubMed: 9809557]
3. Mu Y, Gage FH, Adult hippocampal neurogenesis and its role in Alzheimer's disease. Molecular neurodegeneration 6, 85–93 (2011). [PubMed: 22192775]
4. Crews L et al., Increased BMP6 levels in the brains of Alzheimer's disease patients and APP transgenic mice are accompanied by impaired neurogenesis. J Neurosci 30, 12252–12262 (2010). [PubMed: 20844121]
5. Gomez-Nicola D et al., Temporal dynamics of hippocampal neurogenesis in chronic neurodegeneration. Brain 137, 2312–2328 (2014). [PubMed: 24941947]
6. Jin K et al., Increased hippocampal neurogenesis in Alzheimer's disease. Proceedings of the National Academy of Sciences of the United States of America 101, 343–347 (2004). [PubMed: 14660786]
7. Li B et al., Failure of neuronal maturation in Alzheimer disease dentate gyrus. J Neuropathol Exp Neurol 67, 78–84 (2008). [PubMed: 18091557]
8. Lovell MA, Geiger H, Van Zant GE, Lynn BC, Markesbery WR, Isolation of neural precursor cells from Alzheimer's disease and aged control postmortem brain. Neurobiology of aging 27, 909–917 (2006). [PubMed: 15979211]
9. Perry EK et al., Neurogenic abnormalities in Alzheimer's disease differ between stages of neurogenesis and are partly related to cholinergic pathology. Neurobiology of disease 47, 155–162 (2012). [PubMed: 22504537]
10. Oakley H et al., Intraneuronal beta-amyloid aggregates, neurodegeneration, and neuron loss in transgenic mice with five familial Alzheimer's disease mutations: potential factors in amyloid plaque formation. J Neurosci 26, 10129–10140 (2006). [PubMed: 17021169]
11. Lazarov O et al., Environmental enrichment reduces Abeta levels and amyloid deposition in transgenic mice. Cell 120, 701–713 (2005). [PubMed: 15766532]
12. Radak Z et al., Exercise plays a preventive role against Alzheimer's disease. J Alzheimers Dis 20, 777–783 (2010). [PubMed: 20182027]
13. van Praag H, Kempermann G, Gage FH, Running increases cell proliferation and neurogenesis in the adult mouse dentate gyrus. Nature neuroscience 2, 266–270 (1999). [PubMed: 10195220]
14. Pieper AA et al., Discovery of a proneurogenic, neuroprotective chemical. Cell 142, 39–51 (2010). [PubMed: 20603013]
15. Lie DC et al., Wnt signalling regulates adult hippocampal neurogenesis. Nature 437, 1370–1375 (2005). [PubMed: 16251967]
16. Clelland CD et al., A functional role for adult hippocampal neurogenesis in spatial pattern separation. Science 325, 210–213 (2009). [PubMed: 19590004]
17. Deuker L, Doeller CF, Fell J, Axmacher N, Human neuroimaging studies on the hippocampal CA3 region - integrating evidence for pattern separation and completion. Frontiers in cellular neuroscience 8, 64 (2014). [PubMed: 24624058]

18. Gotz J, Ittner LM, Animal models of Alzheimer's disease and frontotemporal dementia. Nature reviews 9, 532–544 (2008).
19. Meshi D et al., Hippocampal neurogenesis is not required for behavioral effects of environmental enrichment. Nature neuroscience 9, 729–731 (2006). [PubMed: 16648847]
20. Santarelli L et al., Requirement of hippocampal neurogenesis for the behavioral effects of antidepressants. Science 301, 805–809 (2003). [PubMed: 12907793]
21. Garthe A, Behr J, Kempermann G, Adult-generated hippocampal neurons allow the flexible use of spatially precise learning strategies. PloS one 4, e5464 (2009). [PubMed: 19421325]
22. Finch CE, Laping NJ, Morgan TE, Nichols NR, Pasinetti GM, TGF-beta 1 is an organizer of responses to neurodegeneration. Journal of cellular biochemistry 53, 314–322 (1993). [PubMed: 8300749]
23. Flanders KC, Ren RF, Lippa CF, Transforming growth factor-betas in neurodegenerative disease. Progress in neurobiology 54, 71–85 (1998). [PubMed: 9460794]
24. Klassen HJ et al., Expression of cytokines by multipotent neural progenitor cells. Cytokine 22, 101–106 (2003). [PubMed: 12849709]
25. Zhu Y, Ahlemeyer B, Bauerbach E, Krieglstein J, TGF-beta1 inhibits caspase-3 activation and neuronal apoptosis in rat hippocampal cultures. Neurochemistry international 38, 227–235 (2001). [PubMed: 11099781]
26. Battista D, Ferrari CC, Gage FH, Pitossi FJ, Neurogenic niche modulation by activated microglia: transforming growth factor beta increases neurogenesis in the adult dentate gyrus. Eur J Neurosci 23, 83–93 (2006). [PubMed: 16420418]
27. Buckwalter MS et al., Chronically increased transforming growth factor-beta1 strongly inhibits hippocampal neurogenesis in aged mice. Am J Pathol 169, 154–164 (2006). [PubMed: 16816369]
28. Kandasamy M et al., TGF-beta signalling in the adult neurogenic niche promotes stem cell quiescence as well as generation of new neurons. Journal of cellular and molecular medicine 18, 1444–1459 (2014). [PubMed: 24779367]
29. Wachs FP et al., Transforming growth factor-beta1 is a negative modulator of adult neurogenesis. J Neuropathol Exp Neurol 65, 358–370 (2006). [PubMed: 16691117]
30. Choi SH et al., A three-dimensional human neural cell culture model of Alzheimer's disease. Nature 515, 274–278 (2014). [PubMed: 25307057]
31. Cho J et al., Treadmill Running Reverses Cognitive Declines due to Alzheimer Disease. Medicine and science in sports and exercise 47, 1814–1824 (2015). [PubMed: 25574797]
32. Cotman CW, Berchtold NC, Exercise: a behavioral intervention to enhance brain health and plasticity. Trends in neurosciences 25, 295–301 (2002). [PubMed: 12086747]
33. Cotman CW, Berchtold NC, Christie LA, Exercise builds brain health: key roles of growth factor cascades and inflammation. Trends in neurosciences 30, 464–472 (2007). [PubMed: 17765329]
34. Llorens-Martin M, Torres-Aleman I, Trejo JL, Growth factors as mediators of exercise actions on the brain. Neuromolecular Med 10, 99–107 (2008). [PubMed: 18286390]
35. Vaynman SS, Ying Z, Yin D, Gomez-Pinilla F, Exercise differentially regulates synaptic proteins associated to the function of BDNF. Brain Res 1070, 124–130 (2006). [PubMed: 16413508]
36. Wrann CD et al., Exercise induces hippocampal BDNF through a PGC-1alpha/FNDC5 pathway. Cell metabolism 18, 649–659 (2013). [PubMed: 24120943]
37. Hamos JE, DeGennaro LJ, Drachman DA, Synaptic loss in Alzheimer's disease and other dementias. Neurology 39, 355–361 (1989). [PubMed: 2927643]
38. Peng S, Wuu J, Mufson EJ, Fahnestock M, Precursor form of brain-derived neurotrophic factor and mature brain-derived neurotrophic factor are decreased in the pre-clinical stages of Alzheimer's disease. Journal of neurochemistry 93, 1412–1421 (2005). [PubMed: 15935057]
39. Proctor DT, Coulson EJ, Dodd PR, Reduction in post-synaptic scaffolding PSD-95 and SAP-102 protein levels in the Alzheimer inferior temporal cortex is correlated with disease pathology. J Alzheimers Dis 21, 795–811 (2010). [PubMed: 20634587]
40. Rasmussen P et al., In humans IL-6 is released from the brain during and after exercise and paralleled by enhanced IL-6 mRNA expression in the hippocampus of mice. Acta Physiol (Oxf) 201, 475–482 (2011). [PubMed: 21083649]

41. Baier PC, May U, Scheller J, Rose-John S, Schiffelholz T, Impaired hippocampus-dependent and -independent learning in IL-6 deficient mice. Behavioural brain research 200, 192–196 (2009). [PubMed: 19378383]

42. Bowen KK, Dempsey RJ, Vemuganti R, Adult interleukin-6 knockout mice show compromised neurogenesis. Neuroreport 22, 126–130 (2011). [PubMed: 21266900]

43. McPherson CA, Aoyama M, Harry GJ, Interleukin (IL)-1 and IL-6 regulation of neural progenitor cell proliferation with hippocampal injury: differential regulatory pathways in the subgranular zone (SGZ) of the adolescent and mature mouse brain. Brain, behavior, and immunity 25, 850–862 (2011).

44. Vallieres L, Campbell IL, Gage FH, Sawchenko PE, Reduced hippocampal neurogenesis in adult transgenic mice with chronic astrocytic production of interleukin-6. J Neurosci 22, 486–492 (2002). [PubMed: 11784794]

45. Yirmiya R, Goshen I, Immune modulation of learning, memory, neural plasticity and neurogenesis. Brain, behavior, and immunity 25, 181–213 (2011).

46. Zhao C, Deng W, Gage FH, Mechanisms and functional implications of adult neurogenesis. Cell 132, 645–660 (2008). [PubMed: 18295581]

47. Guerrieri D, van Praag H, Exercise-mimetic AICAR transiently benefits brain function. Oncotarget 6, 18293–18313 (2015). [PubMed: 26286955]

48. Kobilo T et al., AMPK agonist AICAR improves cognition and motor coordination in young and aged mice. Learn Mem 21, 119–126 (2014). [PubMed: 24443745]

49. Hong XP et al., Essential role of tau phosphorylation in adult hippocampal neurogenesis. Hippocampus 20, 1339–1349 (2010). [PubMed: 19816983]

50. Horder H et al., Midlife cardiovascular fitness and dementia: A 44-year longitudinal population study in women. Neurology 90, e1298–e1305 (2018). [PubMed: 29540588]

51. Lamb SE et al., Dementia And Physical Activity (DAPA) trial of moderate to high intensity exercise training for people with dementia: randomised controlled trial. BMJ 361, k1675 (2018). [PubMed: 29769247]

52. Santos-Lozano A et al., Physical Activity and Alzheimer Disease: A Protective Association. Mayo Clinic proceedings 91, 999–1020 (2016). [PubMed: 27492909]

53. Briley D et al., Preserved neurogenesis in non-demented individuals with AD neuropathology. Scientific reports 6, 27812 (2016). [PubMed: 27298190]

54. Choi SH et al., Non-cell-autonomous effects of presenilin 1 variants on enrichment-mediated hippocampal progenitor cell proliferation and differentiation. Neuron 59, 568–580 (2008). [PubMed: 18760694]

55. West MJ, Gundersen HJ, Unbiased stereological estimation of the number of neurons in the human hippocampus. The Journal of comparative neurology 296, 1–22 (1990). [PubMed: 2358525]

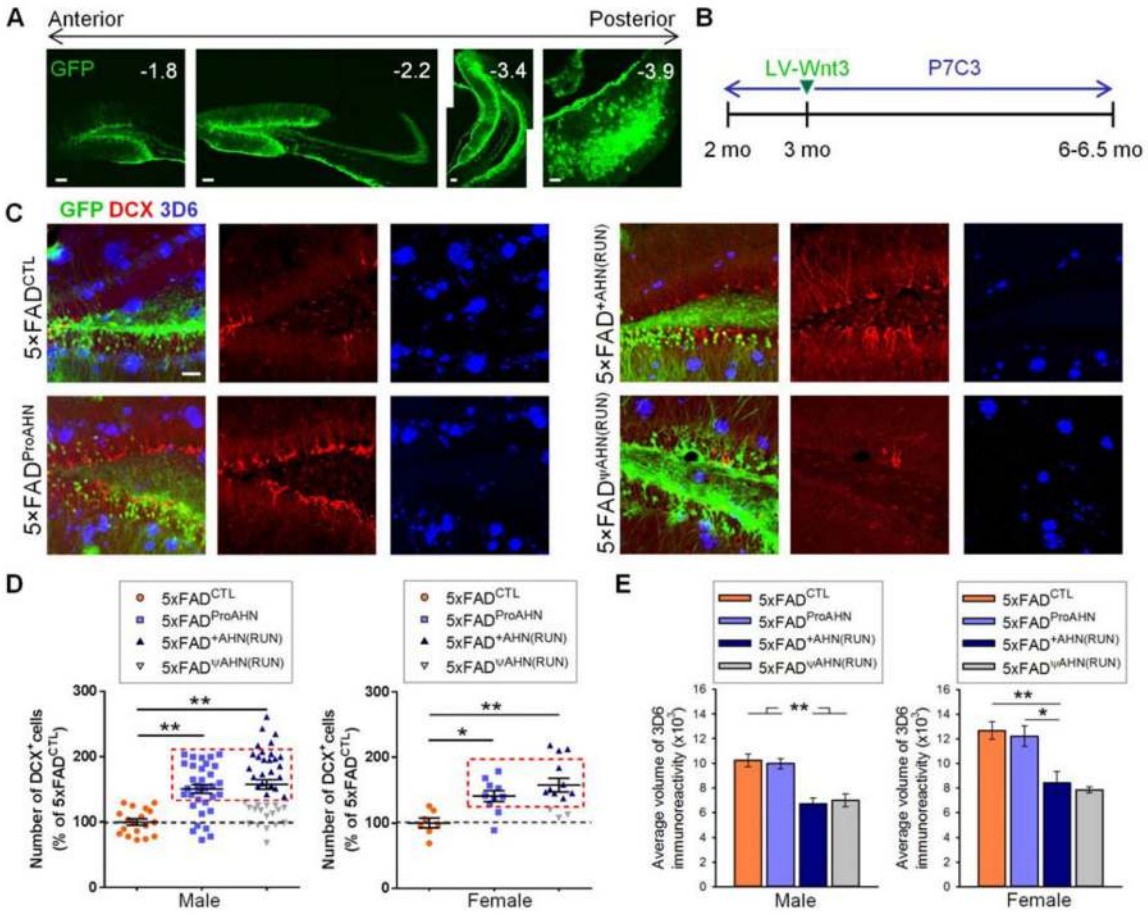

Fig. 1. AHN activation alone does not change Aβ plaque levels.

(**A**) Stereotaxic injection of lentiviral vectors targets adult DG. Numbers (upper right) are approximate distances from bregma. Scale bar: 100 μm. (**B**) Experimental procedures timeline (**C**) Photomicrographs of DCX^+ cells and $3D6^+$ Aβ plaques in the hippocampus of $5\times FAD^{CTL}$, $5\times FAD^{ProAHN}$, $5\times FAD^{+AHN(RUN)}$, and $5\times FAD^{\Psi AHN(RUN)}$ mice. Scale bar: 50 μm. (**D**) Distribution of AHN activation by P7C3 along with LV-Wnt3 or by exercise. Data points represent DCX^+ cell count per mouse, as percentage of mean DCX^+ cell count for $5\times FAD^{CTL}$ mice by gender. In male $5\times FAD^{CTL}$, $5\times FAD^{ProAHN}$, and $5\times FAD^{RUN}$ mice, $F_{(2,90)} = 13.57$, $P < 0.01$. In female, $F_{(2,27)} = 8.05$, $P < 0.01$. (**E**) Quantitative analysis of Aβ burden volume in the hippocampus of $5\times FAD^{CTL}$, $5\times FAD^{ProAHN}$, $5\times FAD^{+AHN(RUN)}$, and $5\times FAD^{\Psi AHN(RUN)}$ mice. Volume in arbitrary units (mean voxel count ± SEM; male, $F_{(3,76)} = 15.57$, $P < 0.01$; female, $F_{(2,19)} = 7.659$, $P < 0.01$). Female $5\times FAD^{\Psi AHN(RUN)}$ mice were excluded due to low n.

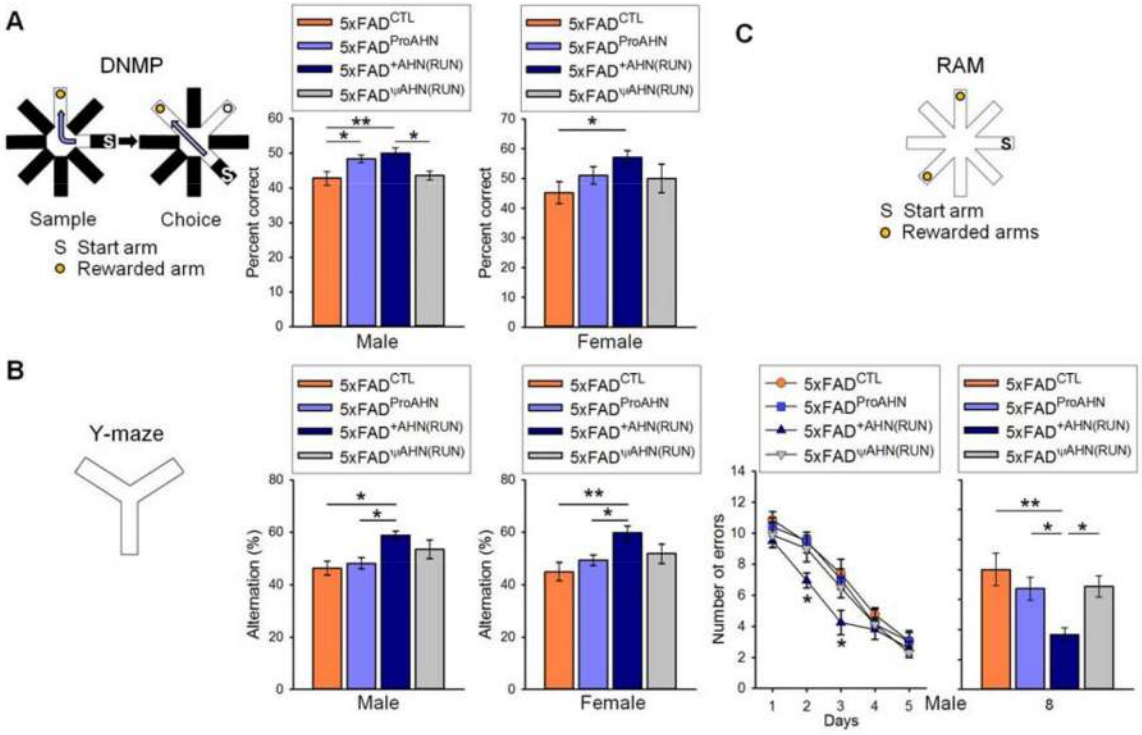

Fig. 2. Increasing AHN alone does not ameliorate cognitive function in 5×FAD mice, whereas exercise-induced AHN does.

(**A**) Schematic of DNMP in RAM task, consisted of sample and choice phase, and quantification of percent correct during choice phase (male, $F_{(3,31)} = 5.983$, $P < 0.01$; female, $F_{(2,19)} = 3.887$, $P < 0.05$). (**B**) Schematic of Y-maze task and spontaneous alternation behavior (male, $F_{(3,31)} = 3.935$, $P < 0.05$; female, $F_{(2,19)} = 7.416$, $P < 0.01$). Total arm entries were comparable among groups (fig. S4). (**C**) Schematic of RAM task and mean error number in training trials (left graph). 2-way ANOVA with repeated measures revealed significant effects for days ($F_{(4,164)} = 99.29$, $P < 0.01$) and groups ($F_{(3,41)} = 5.129$, $P < 0.01$) but not interaction ($F_{(12,164)} = 0.9894$, $P = 0.4613$). Analysis of error number on each day by Fisher's LSD post hoc tests revealed 5×FAD$^{+AHN(RUN)}$ differed significantly from both 5×FAD^{CTL} and 5×FAD^{ProAHN} mice on days 2 and 3 (day 2, $F_{(3,41)} = 4.074$, $P < 0.05$; day 3, $F_{(3,41)} = 3.499$, $P < 0.05$). Right graph: mean error number in memory retention trial ($F_{(3,41)} = 5.675$, $P < 0.01$).

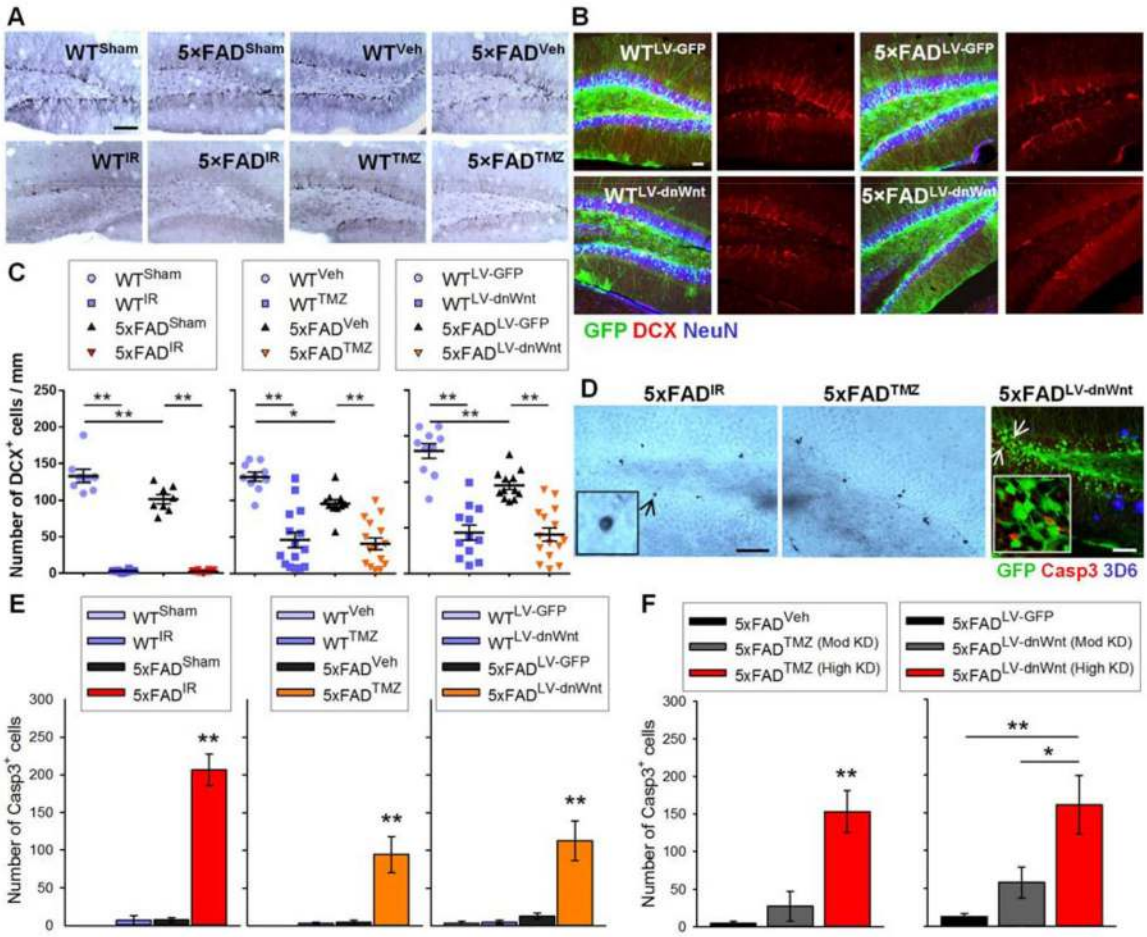

Fig. 3. Ablating AHN induces cell death in 5×FAD mice.

(**A**) Photomicrographs of DCX$^+$ cells in the DG of 5-month-old WT^{Sham}, 5×FAD^{Sham}, WT^{Veh}, 5×FAD^{Veh}, WT^{IR}, 5×FAD^{IR}, WT^{TMZ}, and 5×FAD^{TMZ} mice. Scale bar: 100 μm. (**B**) Photomicrographs of DCX$^+$ cells in the transduced DG of WT and 5×FAD mice by LV-GFP or LV-dnWnt. Mature granule neurons are stained for NeuN. Scale bar: 50 μm. (**C**) Quantification of DCX$^+$ cells in male WT^{Sham}, WT^{IR}, 5×FAD^{Sham}, and 5×FAD^{IR} ($F_{(3,32)}$ = 197.9, P < 0.01; left), WT^{veh}, WT^{TMZ}, 5×FAD^{veh}, and 5×FAD^{TMZ} ($F_{(3,46)}$ = 23.96, P < 0.01; middle), and WT$^{LV\text{-}GFP}$, WT$^{LV\text{-}dnWnt}$, 5×FAD$^{LV\text{-}GFP}$, and 5×FAD$^{LV\text{-}dnWnt}$ mice ($F_{(3,45)}$ = 35.21, P < 0.01; right). (**D**) Representative images of Casp3$^+$ cells in 5×FAD^{IR} (left), 5×FAD^{TMZ} (middle), or 5×FAD$^{LV\text{-}dnWnt}$ (right) mice. Insets represent digital magnification of arrow-indicated Casp3$^+$ cells. Scale bars: 50 μm. (**E**) Quantification of Casp3$^+$ cells in WT^{Sham}, WT^{IR}, 5×FAD^{Sham}, and 5×FAD^{IR} ($F_{(3,32)}$ = 72.38, P < 0.01; left), WT^{Veh}, WT^{TMZ}, 5×FAD^{Veh}, and 5×FAD^{TMZ} ($F_{(3,46)}$ = 11.26, P < 0.01; middle), and WT$^{LV\text{-}GFP}$, WT$^{LV\text{-}dnWnt}$, 5×FAD$^{LV\text{-}GFP}$, and 5×FAD$^{LV\text{-}dnWnt}$ mice ($F_{(3,45)}$ = 11.98, P < 0.01; right). (**F**) Quantification of Casp3$^+$ cells in 5×FAD^{Veh}, 5×FAD$^{TMZ\ (Mod\ KD)}$, and 5×FAD$^{TMZ\ (High\ KD)}$ ($F_{(2,22)}$ = 19.41, P < 0.01; left), and 5×FAD$^{LV\text{-}GFP}$, 5×FAD$^{LV\text{-}dnWnt\ (Mod\ KD)}$, and 5×FAD$^{LV\text{-}dnWnt\ (High\ KD)}$ mice ($F_{(2,24)}$ = 12.17, P < 0.01; right).

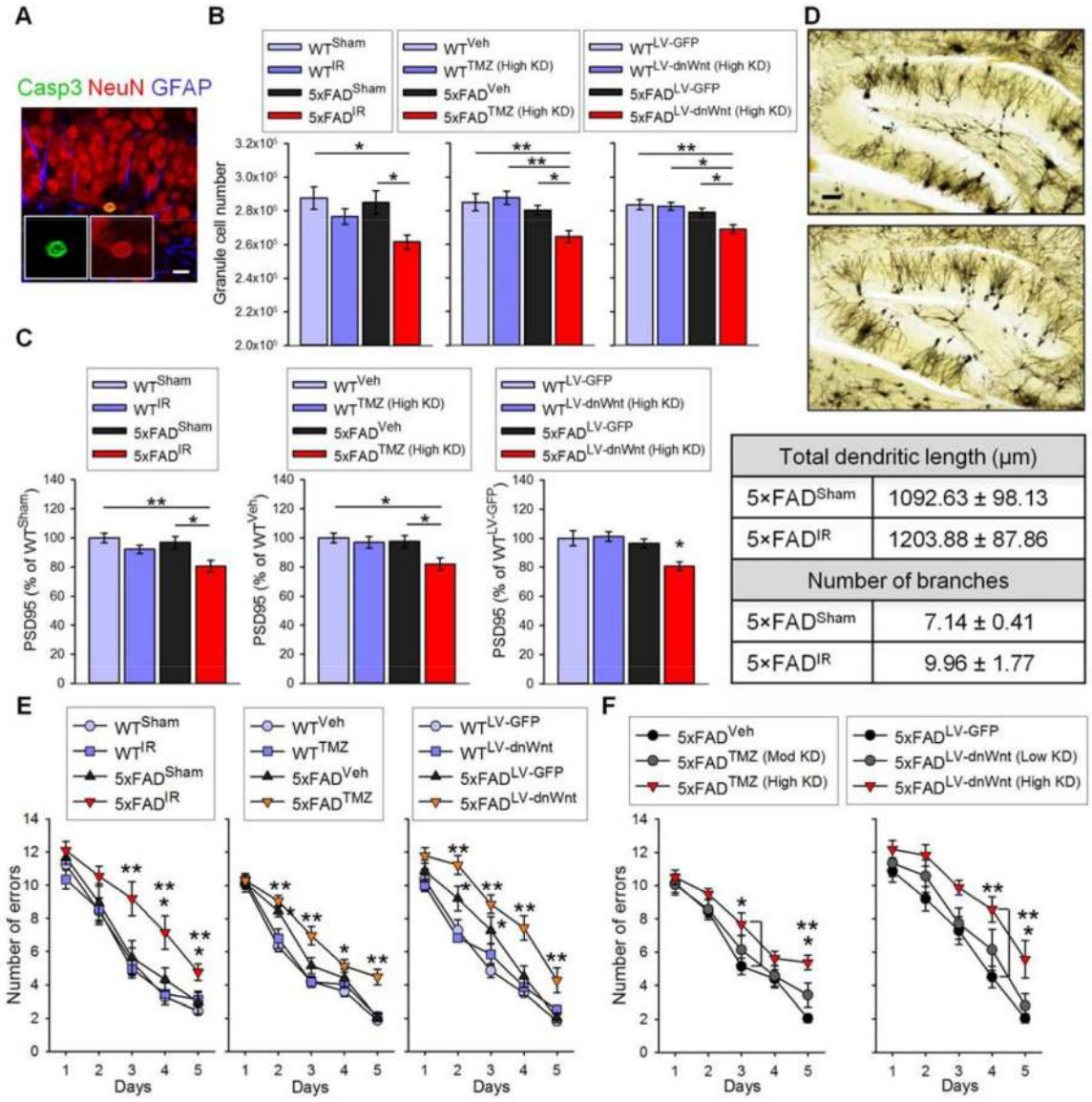

Fig. 4. Ablating AHN induces granule cell and synaptic marker loss, and exacerbates cognitive impairment in 5×FAD mice.

(**A**) Representative images of Casp3^{+} cell colabeled with NeuN. Scale bar: 10 μm. (**B**) Quantification of granule cell number in WT^{Sham}, WT^{IR}, 5×FAD^{Sham}, and 5×FAD^{IR} ($F_{(3,32)}$ = 4.658, P < 0.01; left), WT^{Veh}, WT$^{TMZ\ (High\ KD)}$, 5×FAD^{Veh}, and 5×FAD$^{TMZ\ (High\ KD)}$ ($F_{(3,33)}$ = 6.041, P < 0.01; middle), and WT$^{LV\text{-}GFP}$, WT$^{LV\text{-}dnWnt\ (High\ KD)}$, 5×FAD$^{LV\text{-}GFP}$, and 5×FAD$^{LV\text{-}dnWnt\ (High\ KD)}$ mice ($F_{(3,33)}$ = 5.476, P < 0.01; right). (**C**) Hippocampal PSD95 levels (left: $F_{(3,32)}$ = 5.753, P < 0.01; middle: $F_{(3,33)}$ = 3.983, P < 0.05; right: $F_{(3,33)}$ = 4.639, P < 0.01). (**D**) Representative Golgi stains in 5×FAD^{Sham} (upper) and 5×FAD^{IR} (lower) mice, and quantification of total dendritic length and neuron branch number in outer granule cell layer of 5×FAD^{Sham} (n = 3) and 5×FAD^{IR} mice (n = 4). Scale bar: 100 μm. (**E** and **F**) Mean number of errors in training days of RAM task. In (E), left: WT^{Sham}, WT^{IR}, 5×FAD^{Sham}, and 5×FAD^{IR} mice; middle: WT^{veh}, WT^{TMZ}, 5×FAD^{veh}, and 5×FAD^{TMZ}

mice; right: $WT^{LV\text{-}GFP}$, $WT^{LV\text{-}dnWnt}$, $5\times FAD^{LV\text{-}GFP}$, and $5\times FAD^{LV\text{-}dnWnt}$ mice. In (F), left: $5\times FAD^{Veh}$, $5\times FAD^{tmz\ (Mod\ KD)}$, and $5\times FAD^{tmz\ (High\ KD)}$ mice; right: $5\times FAD^{LV\text{-}GFP}$, $5\times FAD^{LV\text{-}dnWnt\ (Mod\ KD)}$, and $5\times FAD^{LV\text{-}dnWnt\ (High\ KD)}$ mice.

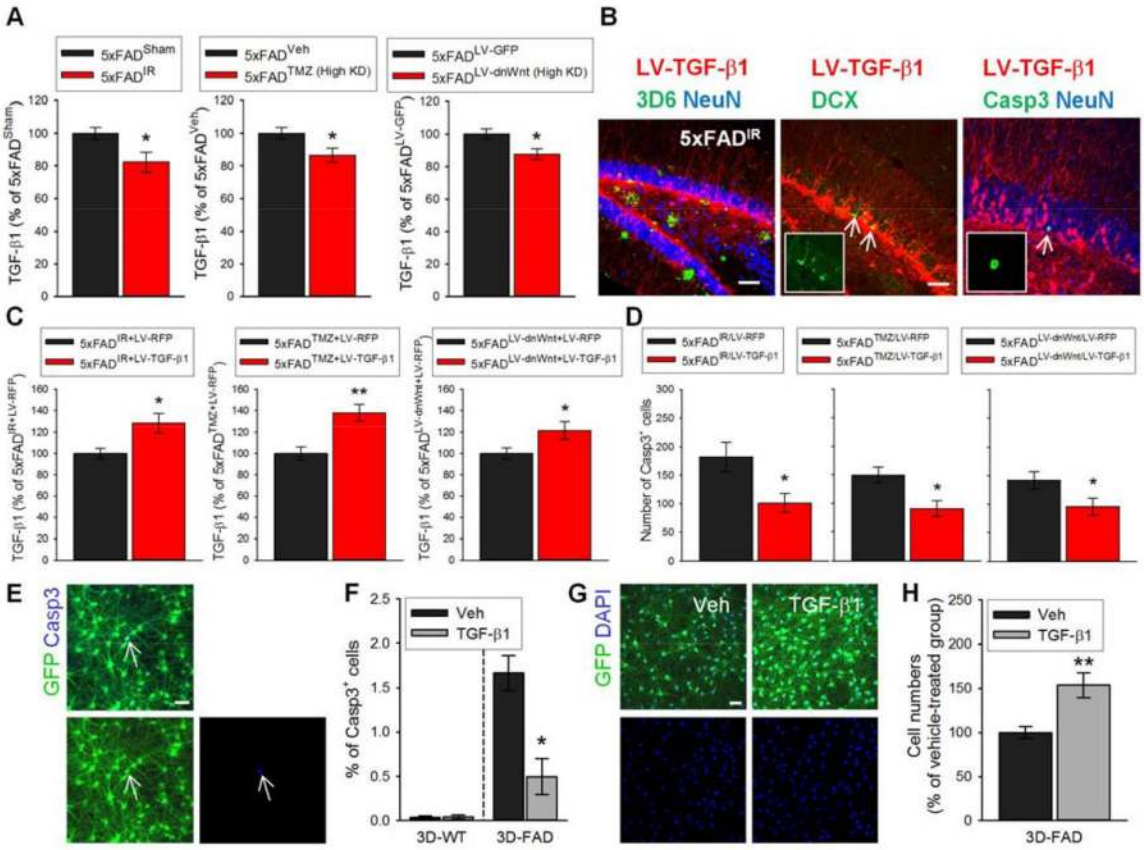

Fig. 5. Ablating AHN in male 5×FAD mice reduces hippocampal levels of TGF-β1, a protective cytokine.

(**A**) Hippocampal TGF-β1 levels in male 5×FAD^{Sham} and 5×FAD^{IR} (left), 5×FAD^{Veh} and 5×FAD$^{TMZ\ (High\ KD)}$ (middle), and 5×FAD$^{LV\text{-}GFP}$ and 5×FAD$^{LV\text{-}dnWnt\ (High\ KD)}$ mice (right). Levels as **%** of 5×FAD control group in each treatment. (**B**) Photomicrographs of 3D6^{+} Aβ plaques and NeuN^{+} cells (left), DCX^{+} cells (middle), and Casp3^{+} cell and NeuN^{+} cells (right) in the transduced DG of 5×FAD^{IR} mice by LV-TGF-β1. Scale bars: 50 μm (left, middle); 20 μm (right). (**C**) Hippocampal TGF-β1 levels in 5×FAD$^{IR/LV\text{-}RFP}$ (n = 8) and 5×FAD$^{IR/LV\text{-}TGF\text{-}β1}$ (n = 8) (left), 5×FAD$^{TMZ/LV\text{-}RFP}$ (n = 9) and 5×FAD$^{TMZ/LV\text{-}TGF\text{-}β1}$ (n = 12) (middle), and 5×FAD$^{LV\text{-}dnWnt/LV\text{-}RFP}$ (n = 8) and 5×FAD$^{LV\text{-}dnWnt/LV\text{-}TGF\text{-}β1}$ (n = 9) (right) mice. Levels as % of 5×FAD control group in each treatment. 5×FAD$^{TMZ/LV\text{-}RFP}$ and 5×FAD$^{LV\text{-}dnWnt/LV\text{-}RFP}$ mice with moderate AHN knockdown were not included. (**D**) Quantification of Casp3^{+} cells in 5×FAD$^{IR/LV\text{-}RFP}$ and 5×FAD$^{IR/LV\text{-}TGF\text{-}β1}$ (left), 5×FAD$^{TMZ/LV\text{-}RFP}$ and 5×FAD$^{TMZ/LV\text{-}TGF\text{-}β1}$ (middle), and 5×FAD$^{LV\text{-}dnWnt/LV\text{-}RFP}$ and 5×FAD$^{LV\text{-}dnWnt/LV\text{-}TGF\text{-}β1}$ (right) mice. (**E**) Representative images of Casp3^{+} cells (arrows) in GFP-labeled 3D-FAD cell cultures. Scale bar: 50 μm. (**F**) Quantification of Casp3^{+} cells in 3D-FAD cell cultures treated with vehicle (veh) or TGF-β1 (10 ng/ml). n = 3 per group. (**G**) Representative images of DAPI^{+} cells (blue) in ReN-FAD cell cultures treated with vehicle or TGF-β1. Scale bar: 50 μm. (**H**) Number of cells survived in 3D-FAD cultures treated with vehicle or TGF-β1. n = 3 per group.

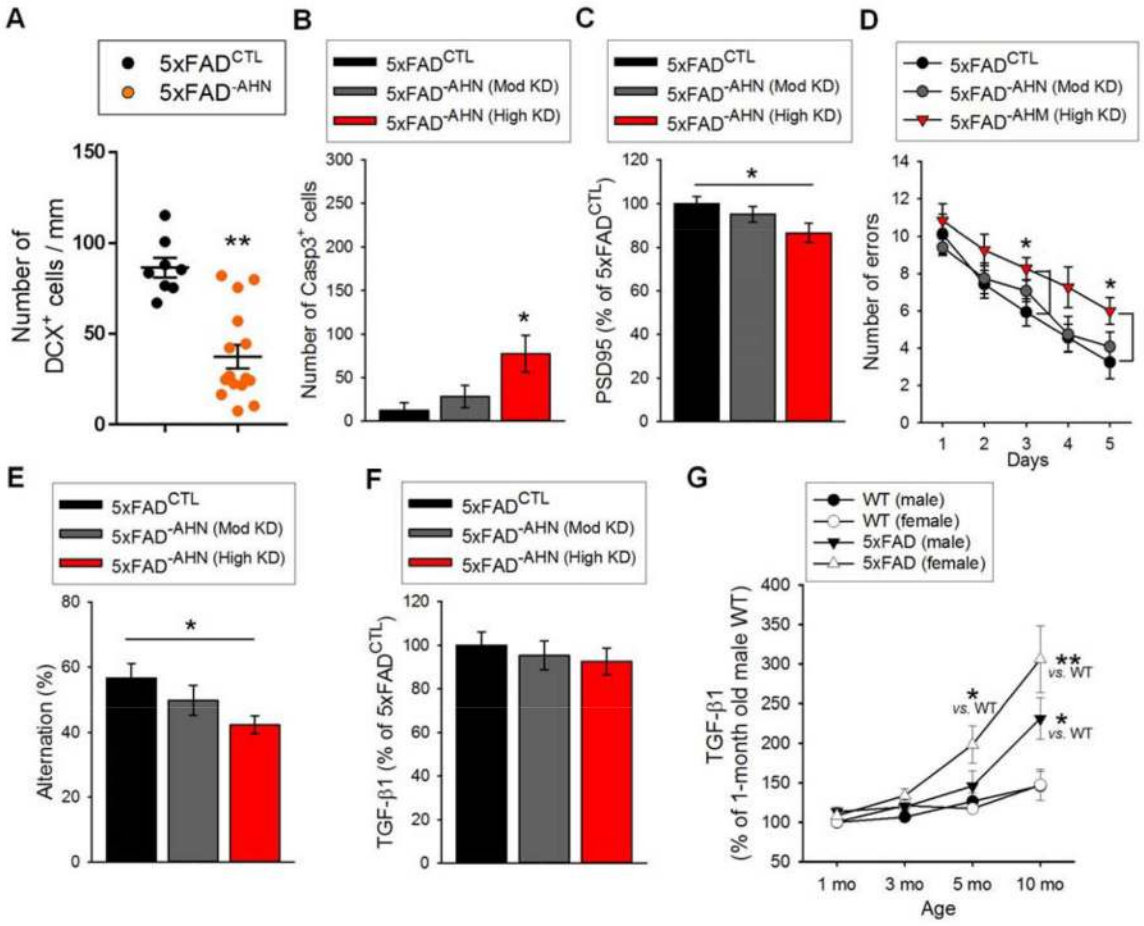

Fig. 6. Effects of ablating AHN in female 5×FAD mice.

(**A**) Quantification of DCX^{+} cells in female 5×FAD^{CTL} and 5×FAD^{-AHN} mice. (**B**) Quantification of Casp3^{+} cells in female 5×FAD^{CTL}, 5×FAD$^{-AHN\ (Mod\ KD)}$, and 5×FAD$^{-AHN\ (High\ KD)}$ mice ($F_{(2,20)} = 4.803$, $P < 0.05$). (**C**) Levels of hippocampal PSD95 ($F_{(2,20)} = 3.499$, $P < 0.05$). Levels as % of 5×FAD^{CTL} group. (**D**) Mean error number in RAM task training trials. 2-way ANOVA with repeated measures revealed significant effects for days ($F_{(4,80)} = 24.19$, $P < 0.01$) and groups ($F_{(2,20)} = 5.982$, $P < 0.01$) but not interaction ($F_{(8,80)} = 0.4305$, $P = 0.8994$). Analysis of error number on each day by Fisher's LSD post hoc tests revealed 5×FAD$^{-AHN\ (High\ KD)}$ differed significantly from 5×FAD^{CTL} mice on days 3 and 5 (day 3, $F_{(2,20)} = 3.495$, $P < 0.05$; day 5, $F_{(2,20)} = 3.419$, $P = 0.0428$). (**E**) Spontaneous alternation in Y-maze ($F_{(2,20)} = 3.747$, $P < 0.05$). Total arm entries comparable among groups (fig. S18G). (**F**) Hippocampal TGF-β1 levels. Levels as % of 5×FAD^{CTL} group. (**G**) Changes in TGF-β1 levels in the hippocampal homogenates of untreated male and female WT and 5×FAD mice with age (n = 7 per group). In 5-month-olds, *P < 0.05 between female 5×FAD and WT mice. In 10-month-olds, *P < 0.05 between male 5×FAD and WT mice; **P < 0.01 between female 5×FAD and WT mice.

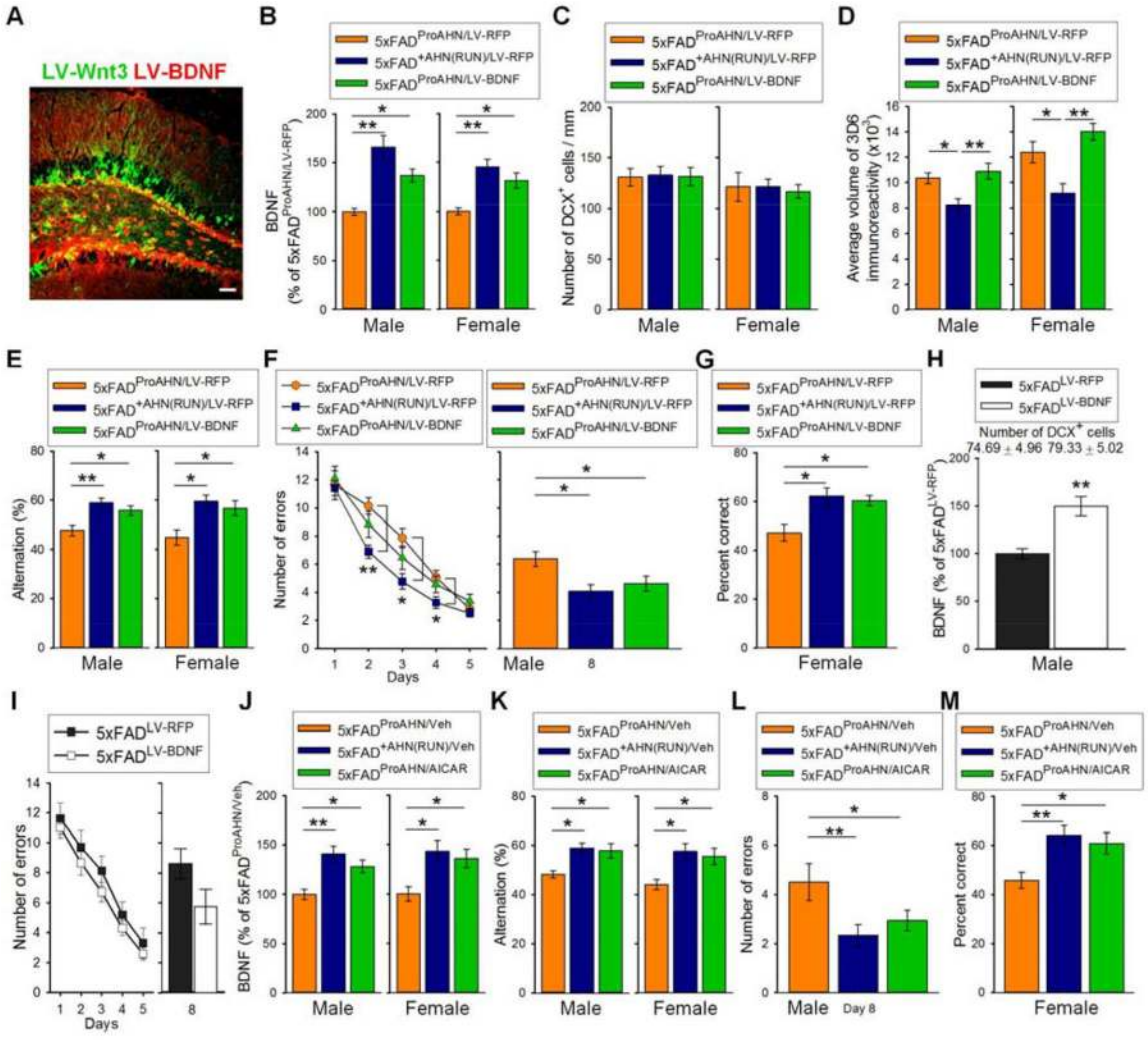

Fig. 7. AHN activation combined with increased BDNF levels ameliorates cognitive function in 5×FAD mice.

(**A**) Photomicrograph of lentiviral expression of LV-Wnt3 and LV-BDNF in the DG of 5×FAD$^{ProAHN/LV-BDNF}$ mice. Scale bar: 50 μm. (**B**) Hippocampal BDNF levels in 5×FAD$^{ProAHN/LV-RFP}$, 5×FAD$^{+AHN(RUN)/LV-RFP}$, and 5×FAD$^{ProAHN/BDNF}$ mice. (**C**) DCX^{+} cell quantification. (**D**) Quantitative analysis of Aβ burden volume (mean voxel count ± SEM). (**E**) Spontaneous alternation behavior in Y-maze task. Total arm entries comparable among groups (fig. S19). (**F**) Left: mean error number for each group (male 5×FAD$^{ProAHN/LV-RFP}$, 5×FAD$^{+AHN(RUN)/LV-RFP}$, and 5×FAD$^{ProAHN/BDNF}$) in RAM task training days. Right: mean error number in memory retention trial. (**G**) Quantification of percent correct during choice phase of DNMP task among female 5×FAD$^{ProAHN/LV-RFP}$, 5×FAD$^{+AHN(RUN)/LV-RFP}$, and 5×FAD$^{ProAHN/LV-BDNF}$ mice. (**H**) Hippocampal BDNF levels in male 5×FAD^{LV-RFP} (n = 8) and 5×FAD$^{LV-BDNF}$ (n = 12) mice. DCX^{+} cell number listed above graph. (**I**) Mean error number in RAM task training trials (left) and mean error number in memory retention trial (right). (**J**) Hippocampal BDNF levels in 5×FAD$^{ProAHN/Veh}$, 5×FAD$^{+AHN(RUN)/Veh}$, and 5×FAD$^{ProAHN/AICAR}$ mice. (**K**) Spontaneous

alternation behavior in Y-maze task. Total arm entries comparable among groups (fig. S21B). (**L**) Mean error number in memory retention trial of RAM task. (**M**) Quantification of percent correct during choice phase of DNMP task among female 5×FAD$^{ProAHN/Veh}$, 5×FAD$^{+AHN(RUN)/Veh}$, and 5×FAD$^{ProAHN/AICAR}$ mice.

Table 1.

Levels of hippocampal BDNF, PSD95, SYP, IL-6, and FNDC5 of male 5×FAD^{CTL}, 5×FAD^{ProAHN}, 5×FAD$^{+AHN(RUN)}$, and 5×FAD$^{∓AHN(RUN)}$ mice.

Animal numbers in parentheses (female mice in Table S7). $F_{(3,31)} = 11.48$, $P < 0.01$ (BDNF); $F_{(3,41)} = 6.279$, $P < 0.01$ (PSD95); $F_{(3,41)} = 6.083$, $P < 0.01$ (SYP); $F_{(3,41)} = 6.047$, $P < 0.01$ (IL-6); $F_{(3,31)} = 5.974$, $P < 0.01$ (FNDC5).

	5×FAD^{CTL}	5×FAD^{ProAHN}	5×FAD$^{+AHN(RUN)}$	5×FAD$^{∓AHN(RUN)}$
BDNF	100.00 ± 5.72 (8)	91.32 ± 3.80 (10)	149.74 ± 10.65** (8)	145.29 ± 13.09** (9)
PSD95	100.00 ± 7.07 (10)	103.19 ± 5.64 (15)	129.39 ± 6.47* (12)	128.23 ± 4.41* (8)
SYP	100.00 ± 6.02 (10)	102.03 ± 4.21 (15)	125.59 ± 7.04* (12)	125.02 ± 4.39* (8)
IL-6	100.00 ± 2.58 (10)	105.44 ± 3.86 (15)	128.89 ± 9.80* (12)	129.52 ± 6.74* (8)
FNDC5	100.00 ± 6.54 (8)	100.16 ± 7.49 (10)	131.78 ± 6.26* (8)	127.41 ± 7.03* (9)

* $P < 0.05$;

** $P < 0.01$ compared to 5×FAD^{CTL} and 5×FAD^{ProAHN} mice.